ADVANCED IMPINGEMENT COOLING WITH NOVEL SURFACE FEATURES

by

Sarwesh Narayan Parbat

B.Tech, Mechanical Engineering, SRM University, India, 2011

Submitted to the Graduate Faculty of

the Swanson School of Engineering in partial fulfillment

of the requirements for the degree of

Master of Science in Mechanical Engineering

University of Pittsburgh

2015

UNIVERSITY OF PITTSBURGH

SWANSON SCHOOL OF ENGINEERING

This thesis was presented

by

Sarwesh Narayan Parbat

It was defended on

July 13, 2015

and approved by

David Edward Schmidt, Ph. D, Assistant Professor, Departmental of Mechanical Engineering and Materials Science

Sung Kwon Cho, Ph. D, Professor, Departmental of Mechanical Engineering and Materials Science

Thesis Advisor: Minking K Chyu, Ph. D, Professor, Departmental of Mechanical Engineering and Materials Science

ADVANCED IMPINGEMENT COOLING WITH NOVEL SURFACE FEATURES

Sarwesh Narayan Parbat, M.S.

University of Pittsburgh, 2015

In the present study four novel surface features have been investigated to study the effects on the heat transfer performance in a narrow rectangular jet impingement channel with channel height–to-jet diameter ratio H/D = 2. The features studied are non-spherical dimples on target plate, chevron elements extending the full channel height, 90^o ribs and 45^o wedges on the jet issuing plate. The transient liquid crystal technique was used to measure the heat transfer coefficient on the impingement plate at four different Reynolds numbers ranging from 61,000 to 97,000. The experimental results were compared to the numerical results obtained through steady state CFD analysis performed using a commercially available software, ANSYS CFX 14.0. The numerical results qualitatively agreed with the heat transfer distribution obtained through experiments, however, the SST turbulence model overpredicted the heat transfer coefficients. It was observed that the configuration with 45^o wedges on the jet issuing plate has the highest heat transfer enhancement among all tested configurations. The dimples and the chevrons offered some restriction to the spreading of the impinging jets which prevented these features from providing expected enhancement. However, each dimple had a high local heat transfer in spanwise averaged heat transfer at the edges. The full height chevron elements did not improve the total averaged heat transfer but the deflection of the jets due to crossflow was minimized. In case of the configurations with 45^o wedges and 90^o ribs installed on the jet issuing plates, heat transfer

enhancement was observed in the downstream side of the last jet. This was because of improved convection caused by diversion of the crossflow towards the target plate.

TABLE OF CONTENTS

LIST OF FIGURES

NOMENCLATURE

Roman Letters

D Jet diameter

D_h Jet channel hydraulic diameter

e Rib Height

f Friction factor, $\left(\frac{\Delta P}{\rho\left(\frac{U2}{2}\right)}\right)\left(\frac{D_h}{L}\right)$

h Heat transfer coefficient (W/m^2-K)

H Jet channel height

k Thermal conductivity of air (W/m.K)

Nu Nusselt number

P Pressure (Pa)

Pr Prandlt number

Re Reynolds number, $\frac{UD_h}{\nu}$

S Jet-to-jet spacing (streamwise)

T Temperature (Celsius)

U Bulk mean velocity of jet channel (m/s)

Greek symbols

ρ Density (kg/m^3)

μ Dynamic viscosity (kg/m.s)

Superscript

◦ Degree

Subscript

o Smooth channel

ACKNOWLEDGEMENTS

I would like to start by thanking Dr. Chyu for accepting to be my research advisor. I have always looked up to him and have learnt a lot from him and his work within the short duration of my MS degree program. I would also like to thank the University of Pittsburgh for providing me with world class coursework and research facilities. I want to extend my gratitude to all the faculty and staff members of the Department of MEMS for guiding and helping me during this journey. Special thanks to Dr. David Schmidt and Dr. Sung Kwon Cho for taking out the time to be on my Masters committee at such a short notice and being patient with the delay in submitting the manuscript. I want to specially thank my mentor, Dr. Sin Chien Siw, for providing me with extensive help and guidance at every step.

Finally, I want to dedicate this work to my parents, Mahesh and Urmila Parbat, my sisters and my grandparents, for believing in me and my dreams and their encouragement, blessings and support.

1.0 INTRODUCTION

1.1 GAS TURBINE COOLING

Gas turbines engines are one of the most important marvels of modern day technology. They are found everywhere, from modern day aircrafts to power plants. The turbine engines have high power-to-weight ratio and thus, they are in use at places where performance is of higher importance. Theses engines are complicated and need to have a very high degree of reliability while performing under harsh and high temperature conditions which exceed the melting point of the metal substrate.

One of the most important factors affecting the lifespan and reliability of a jet engine is the operational temperature of the internal hot gas path components. A higher temperature at the inlet of the rotor is desired to achieve a higher efficiency in order to comply with the performance goal of the future fossil energy power systems and greenhouse gas emission targets [1]. The increase in the turbine inlet temperature with development of advanced cooling schemes and material is shown below in Figure 1.

As can be seen from Figure 1, the present rotor inlet temperature is limited at about 1427^{o}C (2600^{o}F). In the 1950's, the rotor inlet temperature was limited to around 800^{o} C primarily because of the lack of cooling schemes for the blades. Around 1990's, with the development of advanced cooling schemes like film cooling and thermal barrier coating (TBC),

the hot gas path components were able to withstand a higher temperature. limit greater than 1200ºC while the material temperature limit still remained around 900ºC.

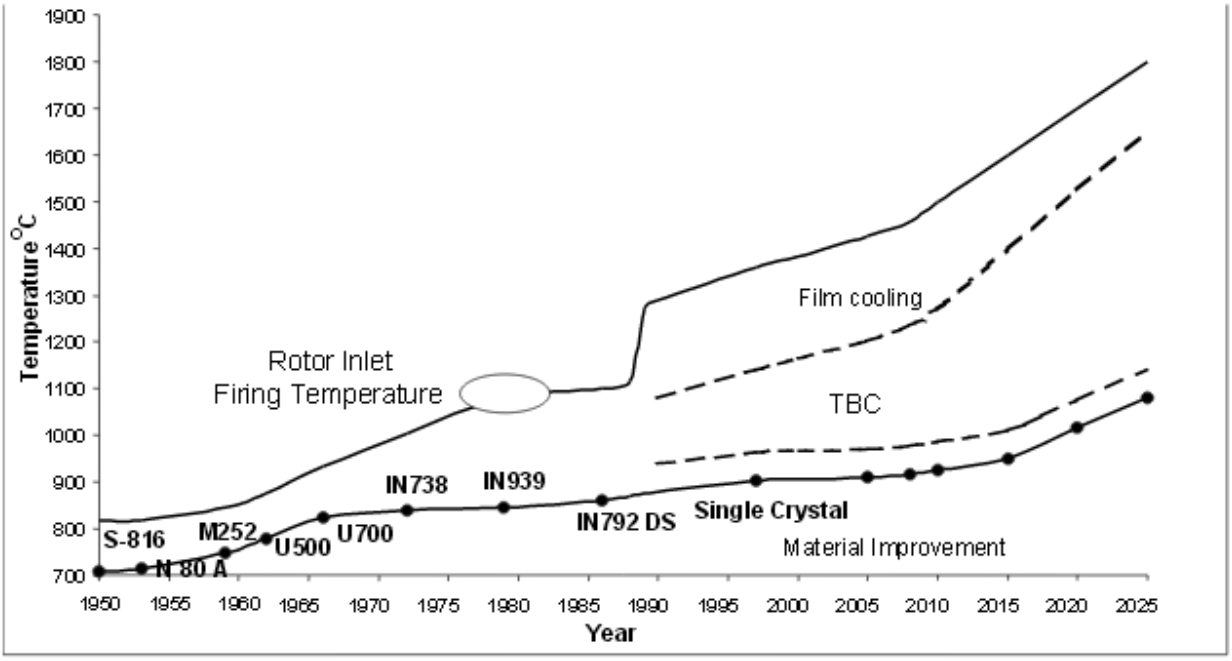

Figure 1. Impact of Firing / Metal Temperature on Efficiency [2]

With a focus on achieving a higher thermal efficiency in near future, the rotor inlet temperature is slated to increase up to approximately 1800º C without a significant improvement in the material temperature limits. Thus, study of advanced cooling schemes have become imperative.

As mentioned earlier, the turbine inlet temperature ranges from 1400˚C to 1800˚C. The temperature limit for the metal substrate used for the turbine components can typically withstand up to about 1000ºC. (Apart from novel newly developed material, and thermal barrier coating, advanced cooling strategies are implemented to ensure the desirable reliability and durability of the turbine engines). As a result, a sophisticated cooling strategies is necessary to ensure desirable reliability and life of the engines. It is very important to be able to predict the temperature distribution in the turbine components. Even a deviation of about 27ºC (50ºF) in

prediction of blade temperature can reduce the life by 50% [3]. Thus, both experimental and numerical techniques are employed to predict temperature profiles which hold for engine like flow conditions.

The primary mode of heat transfer is through convection. Both internal and external cooling schemes are employed to attain the desired temperature limits within the turbine airfoil and to prevent local hot and cold spots. The external cooling schemes include 1) film cooling and 2) use of thermal barrier coating (TBC). The film cooling comprises of spent coolant air which has been used for cooling the internal surfaces of the blade, being ejected from specific locations on the blade profile through bleed holes. Combined with the thermal barrier coating, this relatively cool air forms a thin insulating layer between the external surface of the blade and the hot combustion gases.

The leading edge of the turbine blade considered one of the main section that is exposed to complex flow field and the highest thermal load, which demands high cooling requirements compared to other section, i.e., the mainbody and endwall. Generally, the internal cooling at the leading edge of the blade is attained through jet impingement cooling which by far, provides a very high heat transfer rate, compared to other internal cooling techniques. Eventually, coolant is ejected through the film cooling holes located at the leading edge and the tip sections. The mainbody of the blade is subjected to relatively lower thermal loads. This region is internally cooled using serpentine channel with surface features that serve as vortex generators, such as pin-fins and rib-turbulators. The surface features promote additional turbulence and mixing, thereby, augmenting the heat transfer performance. The spent coolant from the channels is then directed to the trailing edge. The trailing edge is the thinnest section within the blade and typically mounted with pin-fins that serve as bridging structures between the pressure and

suction sides. Pin-fins are arranged in a configurations to maximize the usage of the coolant prior of exiting the blade.

About a decade ago, the double-walled cooling concept was introduced which claims to have a significant cooling performance as compared to that of conventional cooling techniques. Figure 2 shows a general layout of the double-walled cooling scheme. The airfoil wall has narrow cavities which are connected to a central plenum through impingement holes. The coolant impinges on the inner side of the blade wall exposed to hot gases and provides cooling.

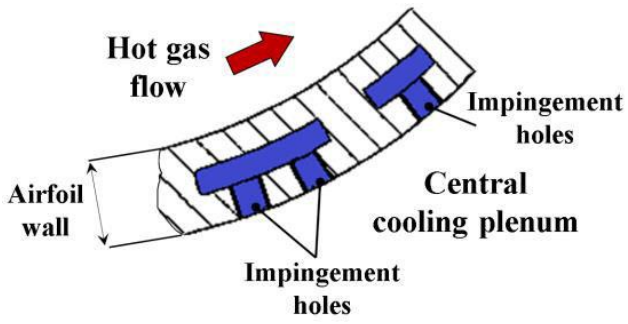

Figure 2. Narrow Impingement Cooling Cavities Within a Turbine Airfoil Wall [4]

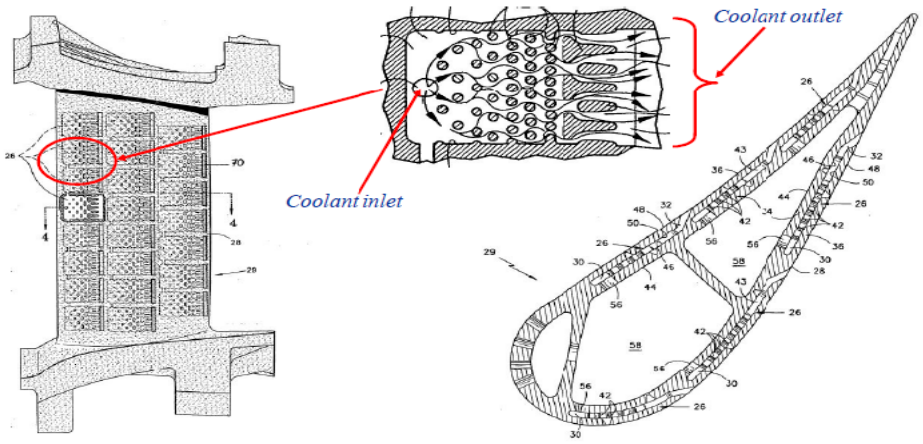

(a)

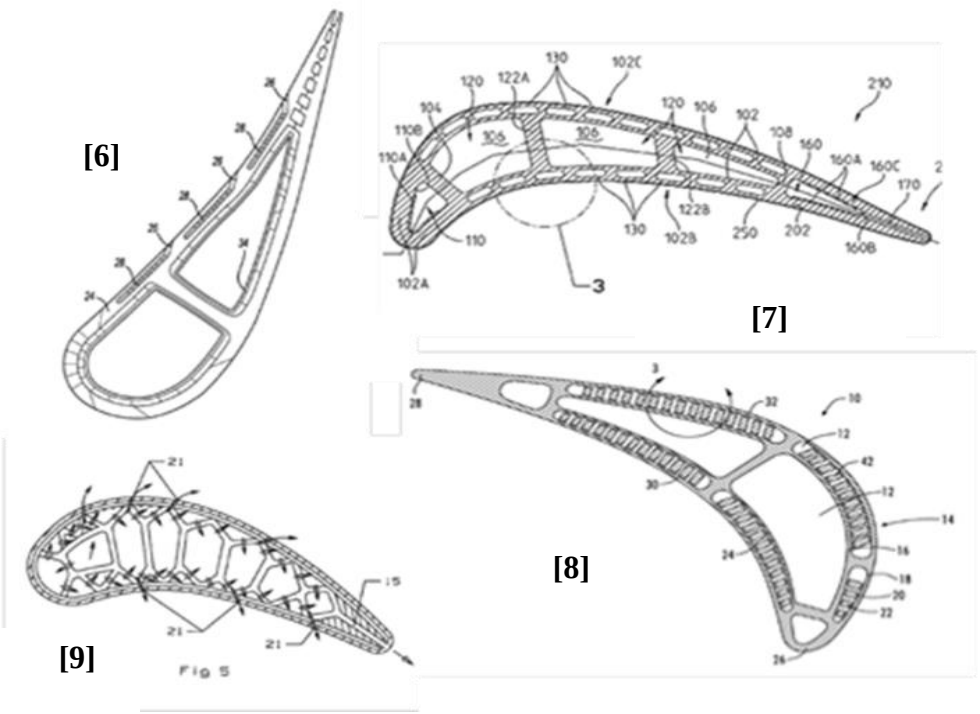

(b)

Figure 3. Double-Walled Cooling Concepts (a) Double-Wall Cooling With Pin-Fins [5] (b) Airfoil With Double-Wall Cooling [6-9]

Figure 3 shows a typical double wall cooling scheme developed by various turbine manufacturers. Note that the cooling channels are positioned closer to the outer walls which can leads to higher removal rate. This integrally cast cooling channels are radially oriented in the turbine airfoil and can be in multiple quantity [4]. These cooling channels can be strategically arranged depending on the cooling demand to achieve uniform temperature distribution within the blade. Since, the jet impingement cooling has very high heat transfer coefficients, the outer wall can be effectively cooled with relatively smaller amount of coolant.

Recent advancement and innovations in the manufacturing technologies and processes have allows the fabrication of internal cooling channels with more complex designs and geometries including the double-walled cooling schemes. The development of additive manufacturing has opened up the doors to practically manufacture such micro level designs in a timely and cost effective manner. The importance of micro cooling was discussed by Bunker [11] who showed that 40% reduction in cooling flow and 50% reduction in thermal stress is achievable. On the other hand, the importance of double wall cooling was shown by Chyu and Alvin [10] and several patents [6 - 9].

1.2 LITERATURE REVIEW OF JET IMPINGMENT COOLING

As mentioned earlier, the leading edge of the blades has the highest thermal load because this region faces the combustion gases coming out from the array of guide vanes. Thus, jet impingement is used to cool this region as it offers the maximum heat transfer rate among all convective cooling schemes. Also, the relatively thicker cross section at the leading edge makes it easier to employ impingement scheme [3]. However, the geometry used for jet impingement

cooling weakens the structure because of the presence of holes. Thus, they are only employed at locations which have highest thermal load [3]. The impingement cooling scheme consists of a perforated plate and two chambers. One of the chambers is pressurized while the other chamber has one or two exit holes which open to the outer environment. The coolant is directed through the perforated plate from the pressurized chamber to the impingement channel due to the existing difference in the static pressure between the chamber and the channel. The orifice present in the perforated plate act as jet nozzles and the pressurized coolant emerges in the form of jets. The coolant then impinges on the opposite wall which is the inner surface of the wall or leading edge providing desired cooling effect. Donovan and Murray [12] showed that at low nozzle to surface spacing (<2 diameters) secondary peaks in the radial heat transfer distributions are due to an abrupt increase in turbulence in the wall jet. It has been shown that at low nozzle to impingement surface spacing, the mean heat transfer distribution in the radial direction exhibits secondary peaks.

Several researchers have studied the parameters affecting the heat transfer performance of jet impingement arrays. Weigand and Spring [13] and Downs and James [14] have discussed various parameters and the effects on the impingement cooling. The crossflow has been cited as one of the most important parameters governing the heat transfer characteristics within the channel. High crossflow in the impingement channel leads to deflection of downstream jet which may cause decrease in the heat transfer rate at the impingement surface as reported by Obot and Trabolt [15]. Van Treuren et al. [16] showed that a distance of 6D between the jet and target surface is required to obtain a fully developed jet. The study looked into the effect of jet-to-plate distance on heat transfer and found that H/D = 2 produces the highest Nusselt numbers. Inline array has been analyzed by Kercher and Tabakoff [17]. They developed a correlation of the heat

transfer performance which included the effects of the crossflow flowing perpendicular to the jets; the effects of the jet diameter, jet spacing, and jet-to-surface distance. Hollworth and Cole [24] showed that deflection in the jets downstream due to crossflow causes a decrease in the heat transfer but higher crossflow may lead to a higher convection heat transfer. Florshuetz et al. [19] also proposed a correlation for jet impingement array with crossflow and pointed out that the inline array has higher heat transfer performance. Chambers et al. [20] studied the effect of initial crossflow and concluded that jets in channels with low jet-to-crossflow velocity ratio were deflected and produced low heat transfer enhancements. A low heat transfer enhancement for the staggered array was reported by Terzis et al [21]. Park et al. [22] explored the effects of high Reynolds number on a jet array impingement cooling. They concluded that the local maximum Nu increases with an increase in the local jet Re but the qualitative distribution remains the same. El-Gabry and Kaminski [23] studied the effect of crossflow on angled jets and found that the heat transfer is lower than the orthogonal jets.

There have been several studies using surface roughness in enhancing heat transfer in impingement cooling. Miller et al. [24] studied the effect of surface roughness of different geometries. They concluded that the presence of ribs can reduce the heat transfer by hindering the impingement. Liu et al. [25] studied both transverse and longitudinal grooves on the target plate. They showed that for a target plate with grooves, the heat transfer is reduced because the impingement flow is hindered.

1.3 PRESENT STUDY

The present work studied the effect of four different surface features on heat transfer rate on the target plate of a narrow impingement channel with channel height to jet diameter ratio, H/D = 2. The surface features investigated were 1) target plate with dimples 2) chevron element which extend from the jet issuing plate to the target plate 3) 45^o wedge and 4) 90^o ribs on the jet issuing plate. The heat transfer rate distribution in each case is compared to the distribution the baseline case which does not have any surface features on either the target or jet issuing plates. The experimental study employs the transient liquid crystal technique. The experiments were conducted using a scaled up test model which simulate the jet channel with five inline jets connected via a plenum. The jet Reynolds number for the experiment were 61,000, 73,000, 85,000 and 97,000 which were obtained by varying the flow rate at the inlet of the plenum.

The dimples were introduced with the motive of promoting turbulence at the target plate. The dimples used in the present work are made up of two geometries merged together 1) a quarter cylinder and 2) an inclined plane, instead of a hemispherical shapes. The jets were made to impinge on the inclined plane and the corresponding heat transfer distribution was recorded.

The chevron elements used had an included angle of 90^o. They were located at a distance of D upstream of jets 2, 3, 4 and 5 and extended through the channel height. The aim was to investigate the shielding effect provided by these elements in an attempt to reduce the crossflow effect on downstream jets.

The 90^o ribs and the 45^0 ribs were installed on the jet issuing plate at a distance D upstream of jets 2, 3, 4 and 5. The ribs and wedges were H/2 in height and width. They extended throughout the width of the channel. The aim of theses design were two folds 1) to provide some shielding to the jet located downstream from each feature and 2) to deflect the cooler air located

in the middle of the channel towards the target plate in order to obtain better convective heat transfer.

The experimental study was supplemented with numerical analysis of the flow domains for each configuration. ANSYS CFX 14.0, which is a commercial CFD package, was used for all the numerical investigation. These studies were aimed at providing better insight into the flow field and flow structures present inside the channel in the different configurations and explain the heat transfer distribution observed.

The comparison between the heat transfer coefficient distribution was carried out by comparing the dimensionless Nusselt number on the target plate for the given Reynolds number. Also, the spanwise averaged heat transfer and total averaged heat transfer for the configurations were compared to the baseline case for each Reynolds number. The pressure drops for each configuration was also compared to the baseline case.

2.0 EXPERIMENTAL SETUP

2.1 TEST SETUP

The overall arrangement of the test setup is shown in Figure 4. The experimental setup consisted of an in-house supply of compressed air, five gate valves, a flow distribution plenum made of Polyvinyl Chloride (PVC) fittings, five digital flow meters, K-Type thermocouples, NI Data recording system connected to a desktop computer, series of inline heaters with variable transformers and a charge-coupled device (CCD) digital camera. The test sections consisted of five different configurations. Each test section is fabricated out of plexiglas because it is transparent and has a low thermal conductivity to ensure the validity of the semi-infinite conduction model that is used to deduce the heat transfer coefficient on the target plate. Figure 5 shows the plenum fed rectangular test section. The plenum is 190.5 mm (7.5 in) x 57.1 mm (2.25 in) x 50.4 mm (2.0 in) in dimensions. The air is fed to the plenum through five inlets. The air then entered the impingement channel through five jet impingement holes, each having a diameter of 9.53 mm (0.375 in), with the inter-jet spacing, S/D of 4. These holes were located on a jet issuing plate which was 19.05 mm (0.75 in) thickness. The rectangular impingement channel is 254 mm (10 in) x 57.15 mm (2.25 in) x 19.05 mm (0.75 in) in dimensions. Thus, the H/D ratio for the channels is 2 for all the tested configurations.

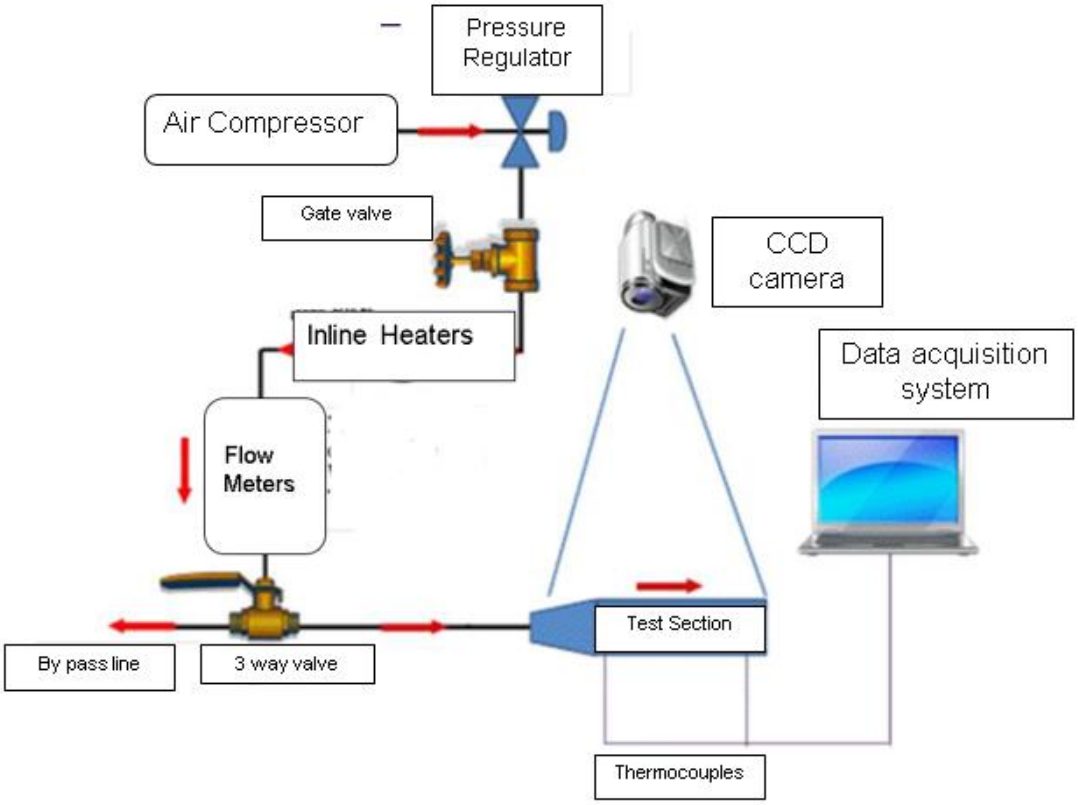

Figure 4. Test Setup Layout

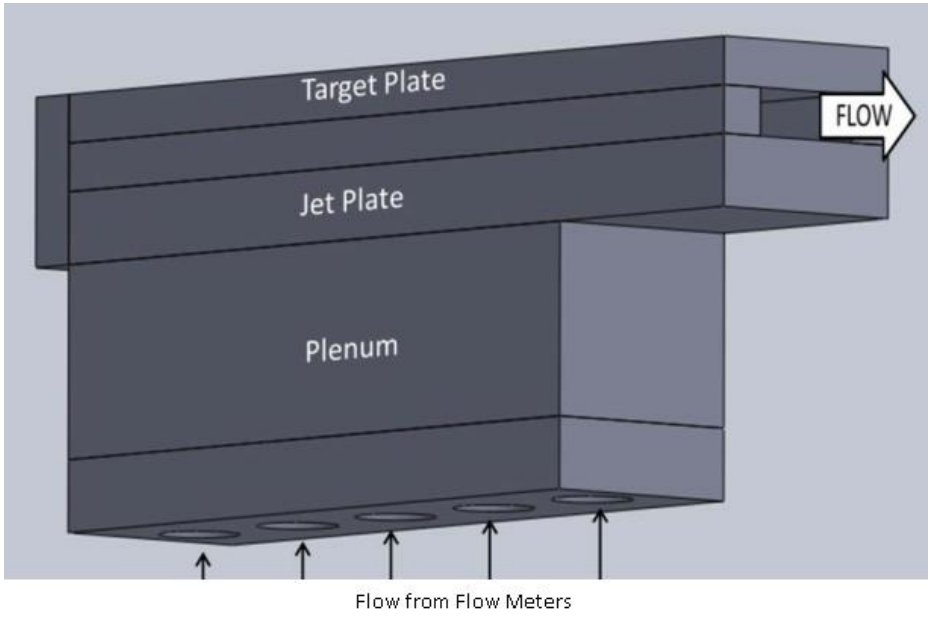

Figure 5. Test Section with Plenum

2.1.1 Baseline Case

The baseline test configuration consisted of a smooth jet impingement channel without any surface features. The data from other test configurations were compared against the baseline case to determine the improvement in the heat transfer rate. The target plate for this configuration was smooth with dimensions 254 mm (10 in) x 57.15 mm (2.25 in) x 12.7 mm (0.5 in).

2.1.2 Dimpulated Target Plate

This configuration had dimples on the impingement side of the target plate, as shown in Figure 6. The primary motive behind the use of dimples on the target plate was to create two different kinds of flow structures at the upstream and downstream edges. Also, the impingement effect should remain unaffected by the crossflow because of the protection offered by the dimple walls around the site of impingement. Each dimple consisted of a pair of an inclined surface and a groove. The diameter of the groove was D. The total projected footprint of the dimple is 19.05 mm (0.75 in) x 31.75 mm (1.25 in). The location of the dimples was set such that the jets impinged at the center of the inclined surface of each dimple.

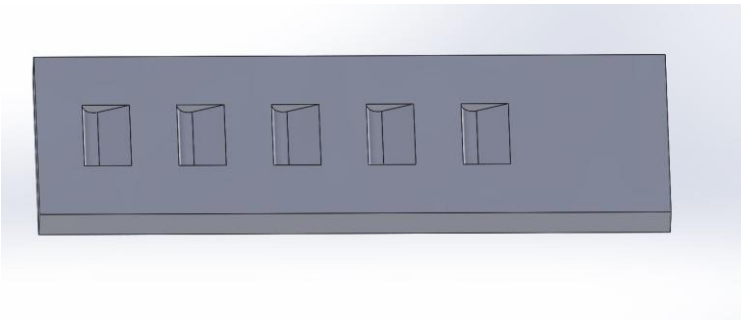

Figure 6. Target Plate with Dimples

2.1.3 Chevron Elements

Figure 7 illustrates the case with right angled chevron elements which were placed at a distance of D upstream of the second jet through the fifth jet. The length of each element was 12.7 mm (0.5 in) and extended from the jet issuing plate up to the target plate. The elements were mounted in place using clear silicon gel in designated groves made in the target plate. The chevron elements are introduced to decrease the crossflow effects on the jets by diverting the crossflow around the jet prior to impingement.

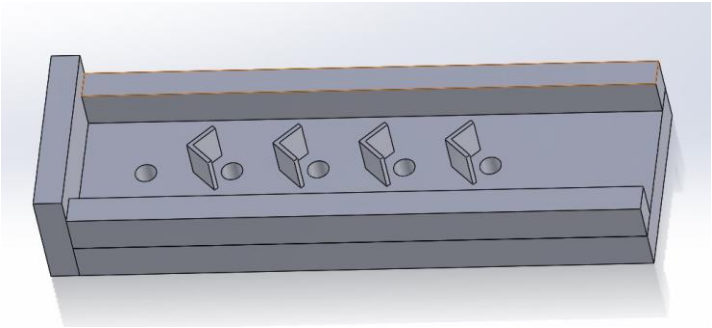

Figure 7. Test Section with Full Length Chevron Elements

2.1.4 Jet Issuing Plate with Ribs and Wedges

In these configurations, two different elements, 90^{o} ribs and 45^{o} wedges are explored. These elements are installed on the jet issuing plate with the motive of deflecting additional coolant towards the target plate, which could eventually result in higher heat transfer. These elements are installed at D/2 distance upstream from the second jet through the fifth jet as illustrated in Figure

8 and Figure 9. The length of the elements is 57.15 mm (2.25 in), same as the width of the channel and the height, e, is 9.53 mm (0.375 in), half the channel height.

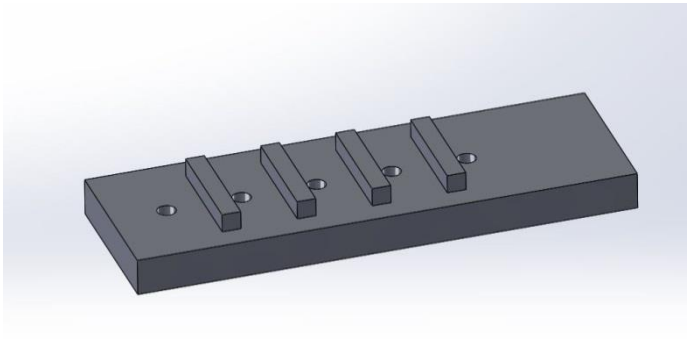

Figure 8. Test Section with 90º Ribs on the Jet Issuing Plate

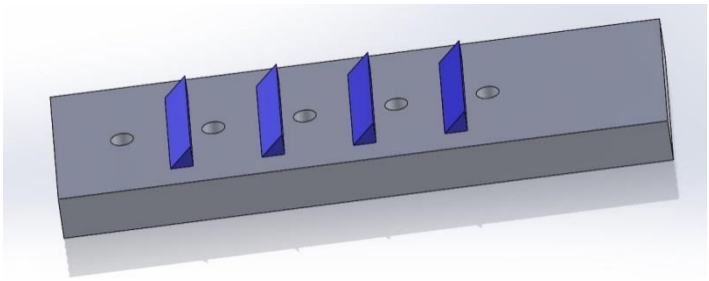

Figure 9. Test Section with 45º Wedges on the Jet Issuing Plate

2.2 EXPERIMENTAL PROCEDURE

The experiments were conducted in the Gas Turbine Heat Transfer Lab at the University of Pittsburgh. The transient liquid crystal technique which was well-documented in the gas turbine community was utilized in this experimental study [26–28]. This technique makes use of

thermochromics liquid crystals which display different color within the selected temperature range. The test surface is sprayed with the liquid crystal layer followed by a layer of black paint using an air brush. The black color backing is used to enhance the color contrast of the liquid crystal during the experiment. This experimental utilized a narrow band liquid crystal, SPNR36C2W, which was purchased from Hall Crest, Inc. The details of this technique can be found in [29].

Compressed air is used from an in-house supply line. The pressure of the air is regulated at approximately 60 psi and passed through an inline heater connected to a variable transformer. This transformer is used to regulate the voltage in order to achieve the desired hot air temperature of approximately 55^{o} C. Initially, the heater is turned off and air at room temperature is allowed to flow through the test section and the valves were adjusted until the desired flow rate is achieved at each of the flow meters. Once the flow is stable, the pressure at the plenum is monitored and measured using a handheld digital manometer. Next, the bypass valves located downstream from the flow meters and upstream from the plenum are opened, thereby, diverting the flow away from the test section. The heater is then turned on and the output of the variable transformer was adjusted to heat the air up to a steady state condition at approximately 55^{o}C. A handheld thermometer with K Type thermocouples is used to monitor the temperature of the air leaving the bypass valves. Once the steady state temperature of about 55^{o} C was obtained, the bypass valves are closed, directing the hot air into the test section. The color history of the liquid crystal layer was recorded using a charge-coupled device (CCD) camera which is mounted perpendicular to the target plate. Simultaneously, the temperature history was recorded using K-Type thermocouples connected to a National Instruments SCXI 1000 Chassis via a National Instruments SCXI 1303 terminal block.

2.3 DATA ANALYSIS

The diameter of the jets for all the configurations was kept constant to main consistency. Thus, the Reynolds number for each case is defined based on the jet diameter. It is assumed that the volumetric flow rate through all the jet is constant and the velocity of flow was obtained based on this assumption. The following relation was used to obtain the Reynolds number.

$$Re = \frac{\rho D U}{\mu} \tag{2.1}$$

For further analysis, the heat transfer coefficients are plotted in terms of Nusselt number, Nu, which is defined as with D_h representing the hydraulic diameter of the jet impingement channel.

$$Nu = \frac{h D_h}{k} \tag{2.2}$$

The heat transfer enhancement, Nu/Nu_0, of each configuration is defined based on the total averaged heat transfer of the target plate, normalized by the fully developed smooth channel, Nu_o, obtained from the Gnielinski correlation, given below

$$Nu_o = \frac{f_o (Re - 1000) Pr}{(1 + 12.7 \left(\frac{f_o}{8}\right) \ \mathrm{Pr}^{\frac{2}{3}} - 1\ )} \tag{2.3}$$

The pressure loss for each configuration is obtained by measuring the static pressure in the plenum using a handheld manometer. The comparison between the pressure drops was done by calculating the friction factor, f, for each case, given by

$$f = \frac{\left(\frac{dp}{dx}\right) D_h}{\frac{\rho U^2}{2}} \tag{2.4}$$

and f_o is calculated using the Petukhov correlation as shown below,

$$f_o = (0.790 \ln Re - 11.64)^{-2} \tag{2.5}$$

$$3000 \leq Re \leq 5\,x10^6 \tag{2.6}$$

The f/f_o was plotted for each case against the Reynolds number so that the pressure drop penalty for each case could easily be compared.

The uncertainty in the measurement of the temperature was 0.5^o C while the uncertainty in the estimation of the Nu number is approximately 8%. The uncertainty in the pressure measurement was estimated to be 7%. The uncertainties are evaluate based on the method proposed by Kline and McClintock [30]. Next, further analysis was performed by comparing the spanwise averaged and total averaged for heat transfer along the channel for all tested configurations. The plots for numerical results were obtained through MATLAB scripts and for the experimental data they were obtained through Liquid Crystal Imaging Analyzer (LCIA), an in-house software.

3.0 NUMERICAL SETUP

All the test configurations are analyzed numerically using ANSYS CFX 14.0. ANSYS CFX is a commercial computational fluid dynamics (CFD) analysis package and is fully implicit in formulation. The fluid domain for the setup is extracted using a commercial CAD package SolidWorks 2014 and consisted of the different jet channel configurations along with the plenum. The Reynolds number, Re_d selected for the purpose of numerical study was 73,000, which corresponded to the flow rate of 18 cubic feet per minute (CFM) per inlet port at the plenum. Steady state simulation is selected over transient simulation because of the limited computation power and time available.

3.1 ANALYSIS SETUP

The boundary conditions are extracted from the experimental data and are shown in Figure 10. The inlet is defined at the five inlet ports of the plenum. A velocity boundary condition is applied to the inlets. The velocity is calculated from the volumetric flow rate readings recorded during the experiments. The density is assumed to be constant. The velocity is applied in the normal direction at the plenum inlet ports. The inlet air is assigned a static temperature of 51.2^o C and medium turbulence intensity of 5% was applied. The surfaces of the target plate, side walls, surface features under investigation and plenum are assigned a constant temperature of 23.5^o C.

Since, all the models are symmetric about the longitudinal axis, a symmetric boundary condition is used in order to decrease the size of the domain and computational costs. At the outlet, a static pressure boundary condition is used with magnitude as atmospheric pressure. The SST turbulence model is selected as it has been shown to provide reasonably acceptable results at lower computational costs as discussed in [31, 32].

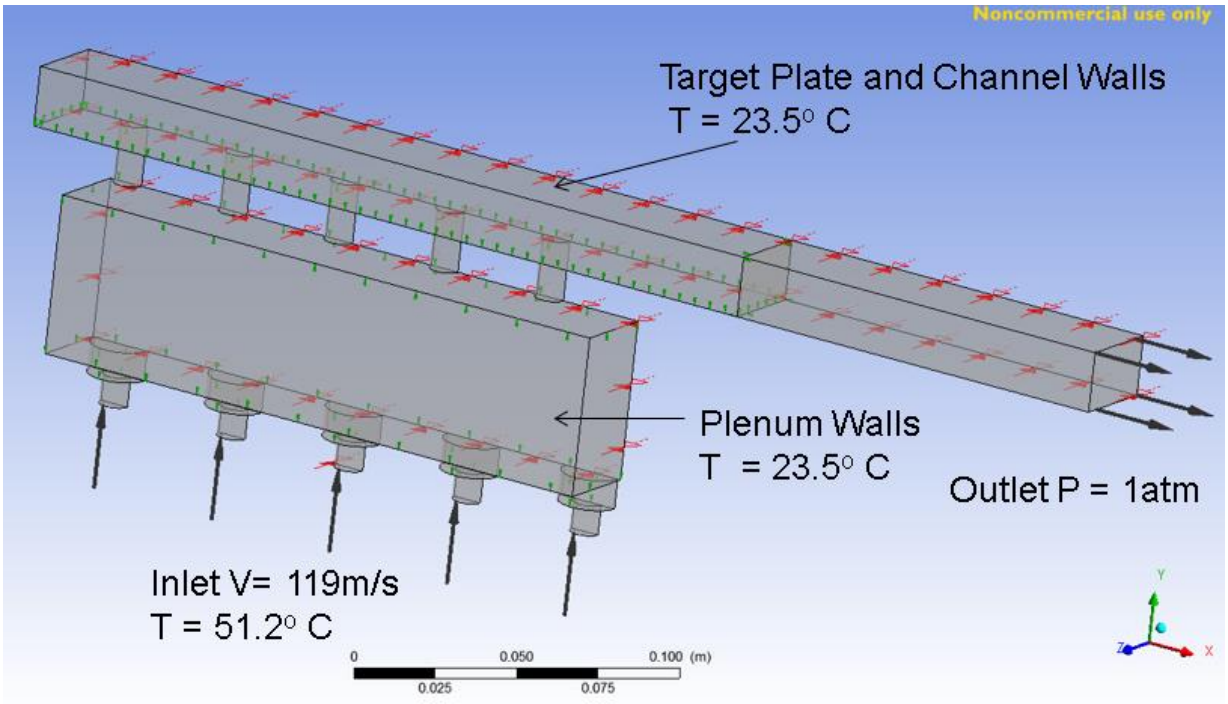

Figure 10. Boundary Conditions for Numerical Analysis for Baseline Fluid Domain (Re = 73,000)

The fluid domain is meshed using the ANSYS Workbench meshing module. Three different mesh densities of approximately 1.2, 2.2 and 4.0 million elements are used to study the grid independence of the obtained solutions. Since, SST turbulence model is used for all the simulations, it is ensured that the y+ values near the walls was less than 2 by using an inflation layer on the solid fluid interfaces. This provide a finer mesh near the walls which resulted in desired y+ values required to capture the detailed phenomena within the boundary layer.

The convergence criteria is set at the maximum RMS of residuals. It was set as 10^{-5} while a conservation convergence criteria of 1 % is used for all the equations. Apart from these, monitor points are assigned at different locations in order to monitor the fluctuations in the variables of interest. These monitor points are set for average and maximum wall heat transfer coefficient for the target plate, the velocity and temperature at the outlet. In cases where convergence criteria are difficult to meet, the fluctuation in these monitor points are observed to confirm convergence.

4.0 RESULTS AND DISCUSSION

4.1 LOCAL HEAT TRANSFER COEFFICIENT DISTRIBUTIONS

The local heat transfer obtained from the experiments for all the configurations at the four different Reynolds numbers used for the experiments are shown in Figure 11–Figure 15. The heat transfer at the jet target plate is largely governed by impingement of the jet on the plate and the effect of the crossflow on the jets downstream. In the present study of channel with jet- to-plate spacing H/D = 2, the heat transfer is seen to be higher at the downstream side. The highest heat transfer occurs at the last jet, Jet 5 and this trend is observed in all the configurations. This trend can be explained in terms of variation of the static pressure in the channel. Air ejected from the jets impinges on the target plate and progresses towards the exit which is located on one side of the channel. This flow of spent air in a direction perpendicular to the jets forms a crossflow. The intensity of crossflow increases downstream because of the addition of spent air from each jet. Since, the cross section of the channel is constant, the velocity of the crossflow will generally increase along the flow direction, thereby, increasing in strength. Due to this increase in velocity, the static pressure in the channel decreases towards the downstream. The plenum, on the other hand, has almost a constant static pressure. As a result, the local pressure difference between jet channel and plenum at each jet increases in the streamwise direction. This causes higher flow

rates in the downstream jets thereby increasing the local Reynolds number which in turn, causes a higher local heat transfer rate compared to the upstream region.

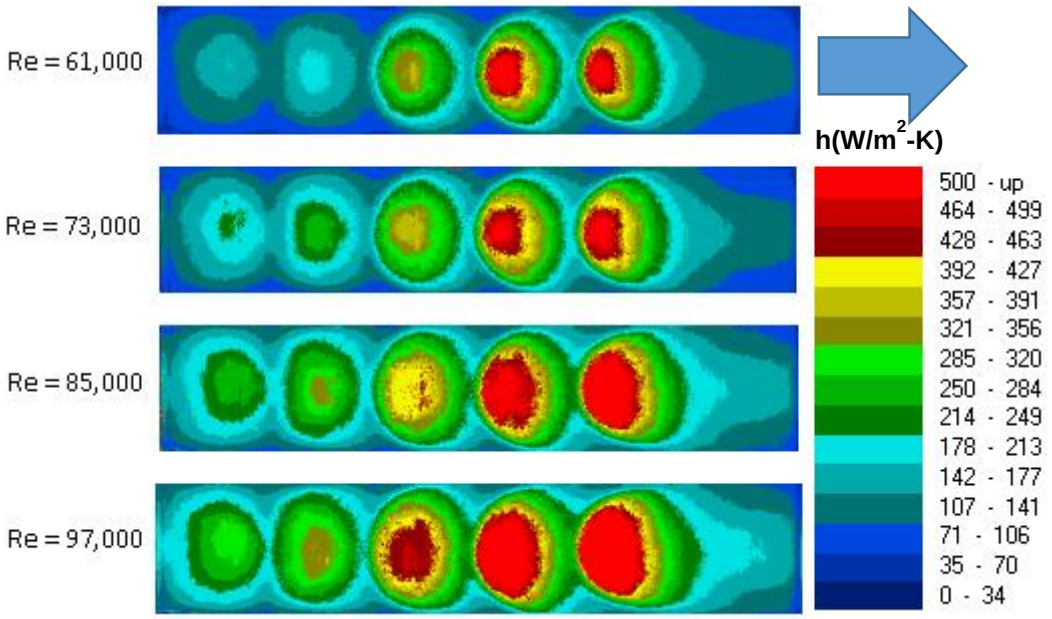

Figure 11. Local Heat Transfer Coefficient Distribution for Baseline Case

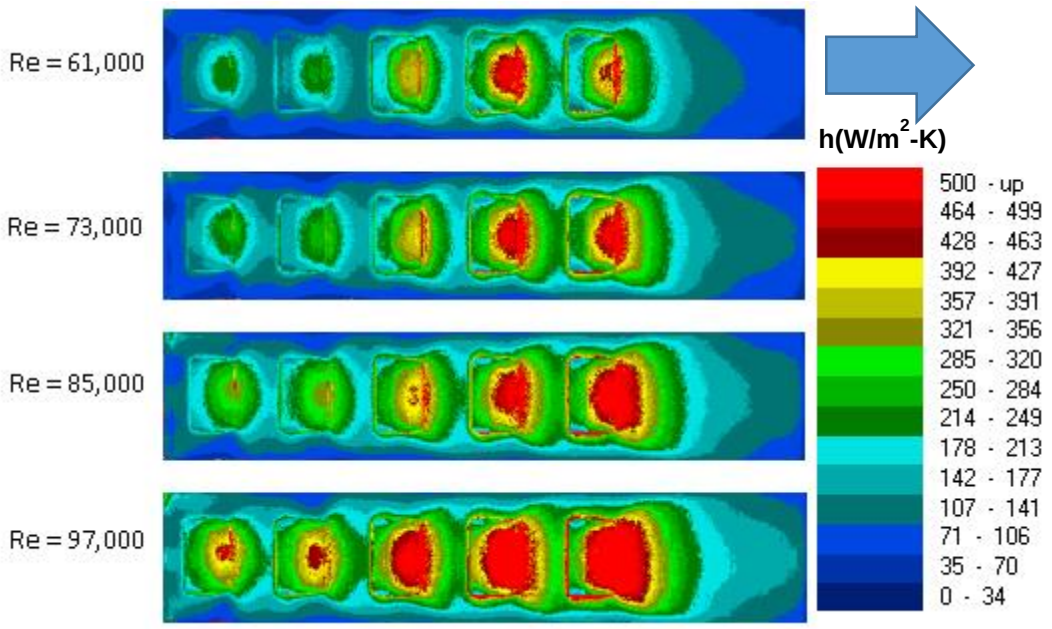

Figure 12. Local Heat Transfer Coefficient Distribution for Dimpulated Target plate

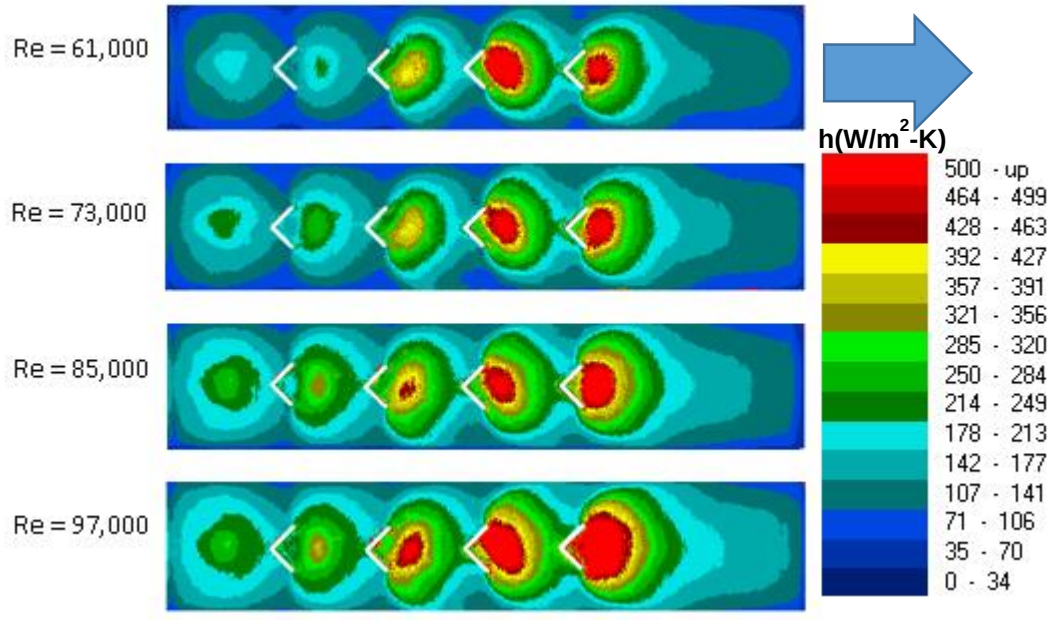

Figure 13. Local Heat Transfer Coefficient Distribution for Test Section with Chevrons

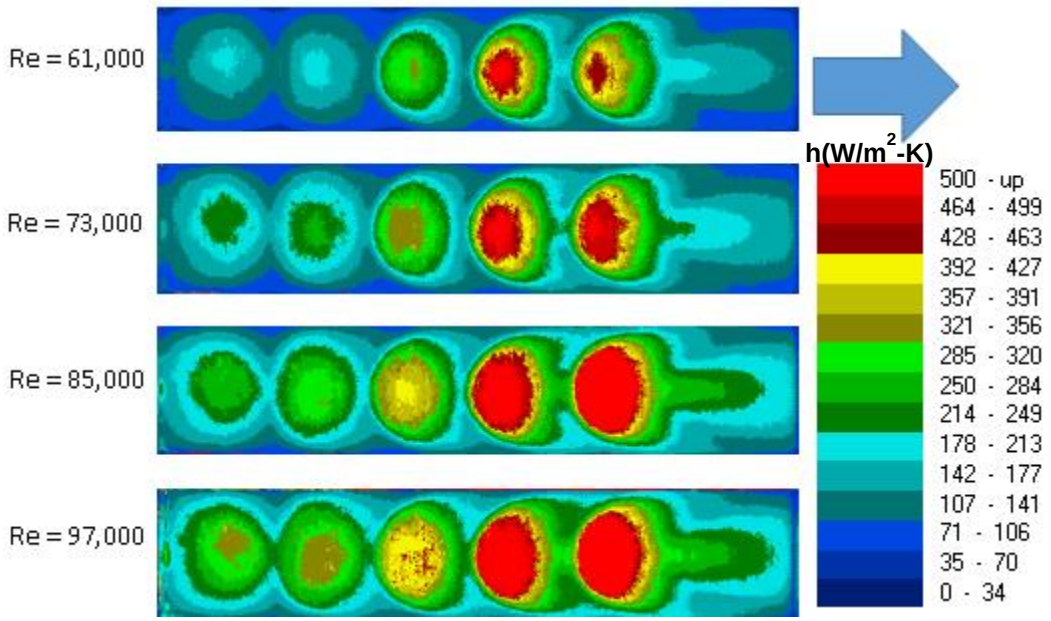

Figure 14. Local Heat Transfer Coefficient Distribution for Test Section with Ribs

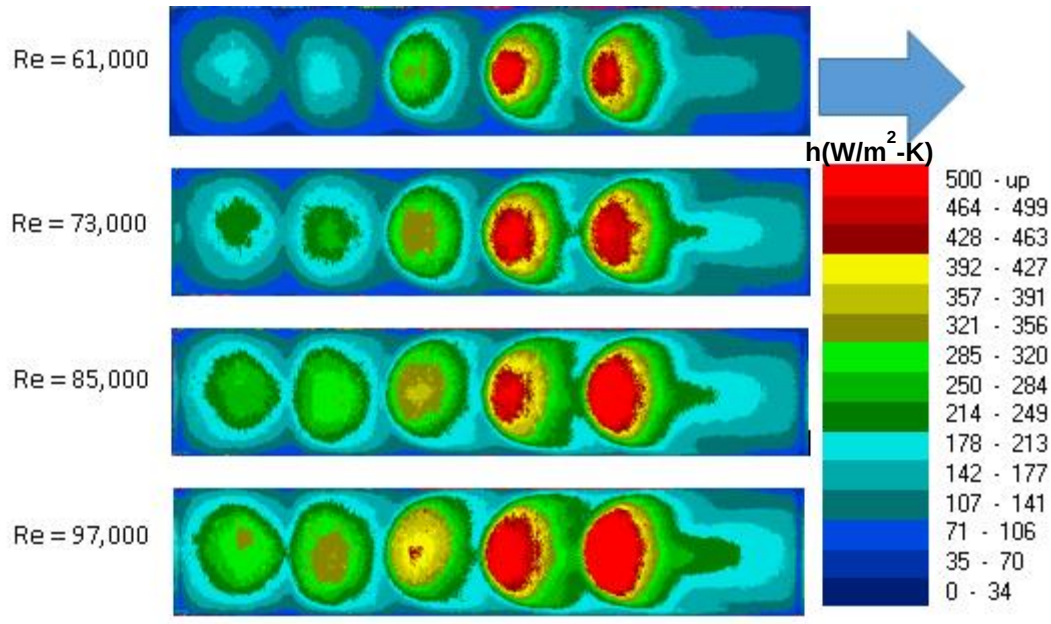

Figure 15. Local Heat Transfer Coefficient Distribution for Test Section with Wedges

Figure 11–Figure 15 illustrate the local heat transfer coefficient distribution of each tested configuration at varying Re ranging between 61,000 up to 97,000. Overall, for all tested configurations, the heat transfer appears to increase along the flow direction. Low heat transfer in the region upstream of the first jet in all the configurations is observed due to the presence of a recirculation zone. In general, the heat transfer at the impingement location depends on the strength of the crossflow and the extent of development of the jet core [33].

For the baseline case, the increase in the local heat transfer rate was observed increase from Jet 1 to Jet 5. The first two jets showed a relatively lower heat transfer due to formation of weaker jets as will be discussed in details in the numerical analysis. The heat transfer at the first, second and the third jets is uniform in the radial direction because of the lower strength of the crossflow. Further downstream, due to the prominent crossflow effects, the heat transfer distribution is similar to a horseshoe vortex formation. The heat transfer at the stagnation points increase with the increase in the Reynolds number as expected.

From the experimental results, it is observed that the flowfield is largely altered by the presence of the dimples on the target plate. After impinging on the inclined surface of the dimple, the jet expands radially in all directions. However, this spreading jet is slowed down because of presence of walls on the leading edge and the sides of the dimple. This causes a decrease in the heat transfer in the front and sides of the dimple cavity. Also, the spreading flow interacts with the dimple cavity walls and is turned away from the target plate, leaving the dimple cavity in a direction parallel to the jets. As a result the flow is separated from the target wall near the dimple edges and is washed away by the crossflow. This phenomenon has twofold effects 1) it reduces heat transfer in the target wall region lying between the dimples and the channel side walls and 2) the separated flow at the edges interacts with the crossflow resulting in

to a very high local heat transfer. On the other hand, the spreading jet is accelerated along the inclined plane in the downstream region of the dimple cavity and is separated from the target wall. This separated flow interacts with the incoming crossflow and causes increase in turbulence and mixing, thereby, causing a very high heat transfer near the trailing edge of the dimples.

In case of the channel with the chevron elements, the stagnation point heat transfer at the all the jets is enhanced as compared to the baseline case. This is because the chevron elements act as a shield and deflect the crossflow away from the jets. This protects the jet core form being deflected by the prevailing crossflow and the impingement is mostly preserved due to negligible deflection. However, the chevron walls prevent the impinging jets from spreading uniformly in the radial direction causing a non-uniform heat transfer distribution. Also, near the chevron walls, the radial flow is slowed down and turned away from the target wall along the chevron length. This causes a recirculation zone and a decrease in the heat transfer between the chevron arms. The deflected crossflow is accelerated because of the smaller cross section area available for flow between the chevron and the channel side walls. Thus, an enhancement in the heat transfer in the downstream of the last jet is observed.

The heat transfer distribution for the configurations with 90^{o} ribs and 45^{o} wedges installed on the jet issuing plate resemble the heat transfer distribution in the baseline case. The first jet in both the configurations shows a higher heat transfer than the baseline. Since, there is no additional geometries on the target plate, the impinging jets spread more uniformly as compared to the configurations with chevron and dimples. With the development of the crossflow, the ribs and the wedges divert more coolant towards the target plate at a higher velocity. This increases the strength of the crossflow near the target plate causing a deflection of the downstream jets. As a result, the third jet has a lower heat transfer. However, this increased

crossflow increases the convective heat transfer and causes a higher heat transfer in the downstream region near the exit for both these configurations.

4.2 SPANWISE AVERAGED HEAT TRANSFER

The spanwise averaged heat transfer distribution on the target plate for all the configurations at jet Reynolds number of 73,000 is shown in Figure 16. The spanwise averaged heat transfer for each configuration is observed to increase in the streamwise direction, being lowest at the first jet and highest at the last jet. This is because the local heat transfer increases in the streamwise direction as already discussed. This trend is common to all the cases which suggest that the heat transfer is largely dominated by the impingement effects.

The spanwise averaged heat transfer for the first jet in all the configurations is comparable. The baseline case has a more uniform heat transfer distribution because there is no restriction to the radial flow of the impinging jets. On the other hand, the chevrons and dimples restricted the radial expansion of the impinging jets. As a result, the spanwise averaged heat transfer for the downstream jets for the baseline case is observed to be higher than the configurations with the chevron elements and the dimples.

For the configuration with dimples on the target plate, regions of very high heat transfer corresponding to the location of edges of the dimples can be seen. As discussed earlier, these are caused because of interaction between the separated flow at the edges of the dimple with the crossflow [25]. The effect of the crossflow can be seen by the deflection of the stagnation point in the downstream direction.

For the test case with chevron elements, the spanwise average heat transfer is the lowest among all tested configurations. This is because the spreading of the jet in radial direction after impingement is restricted due to the presence of the chevron elements that are bringing between the jet issuing plate and the target plate. However, the effect of crossflow is negligible as there is virtually no deflection of the stagnation points.

The configurations with ribs and wedges installed on the jet issuing plate show a trend which is very similar to the baseline case. But the average values for the configuration with ribs is lower than that for the configuration with wedges. The wedges, due to the presence of a 45^{o} inclined face, are able to deflect more coolant towards the target plate, thereby, causing a higher increase in the convective heat transfer as compared to the ribs.

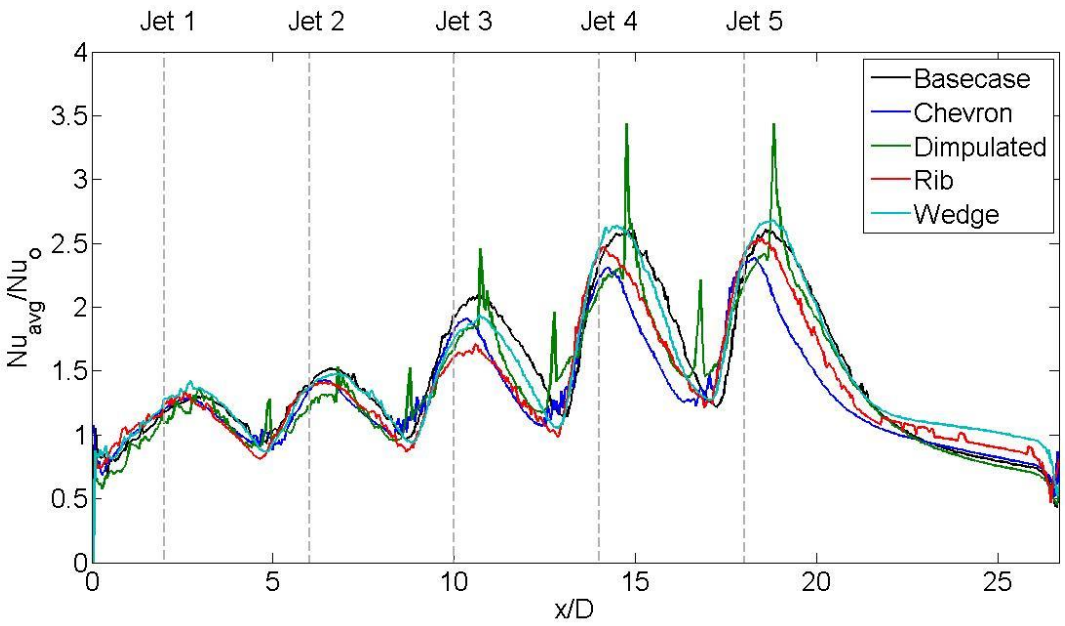

Figure 16. Spanwise Averaged Heat Transfer Distribution

4.3 TOTAL AVERAGED HEAT TRANSFER COEFFICIENT

The total averaged heat transfer coefficient is calculated by averaging the heat transfer coefficients over the entire target plate domain. The results have been discussed in the form of Nusselt number which is calculated for each case and plotted at varying Reynolds numbers. Overall, all tested configuration revealed similar trend that the heat transfer increases with Re. At Re = 61,000, the base case has the highest total average. When the Re increases from 61,000 to 97,000 the baseline case shows the second highest total average heat transfer among all tested configurations. The result revealed that the case with wedges exhibits the highest heat transfer enhancement, followed by the baseline case. The heat transfer performance of the case with dimpulated features and ribs is relatively comparable and slightly lower compared to the baseline case. The case with chevron elements has the lowest heat transfer performance mainly due to the restriction in the radial spreading of the jet .This has ultimately reduces the heat transfer around each individual jet, penalizing the overall heat transfer performance of the channel.

The total heat transfer enhancement is shown in Figure 17 and Figure 18. Figure 17 shows the comparison between the experimental results obtained in present study and the correlation proposed by Florshuetz et al. [19]. The experimental values and the values predicted by the correlation are in good agreement. Figure 18 shows heat transfer based on Nu_{avg} normalized by Nu_o for a channel as obtained by the Gnielinski correlation mentioned earlier. The maximum enhancement achieved is approximately 4.5% in the case of the wedges while all other configurations showed a lower total averaged heat transfer when compared to the baseline case. Overall, the heat transfer enhancement is relatively constant within the tested Re.

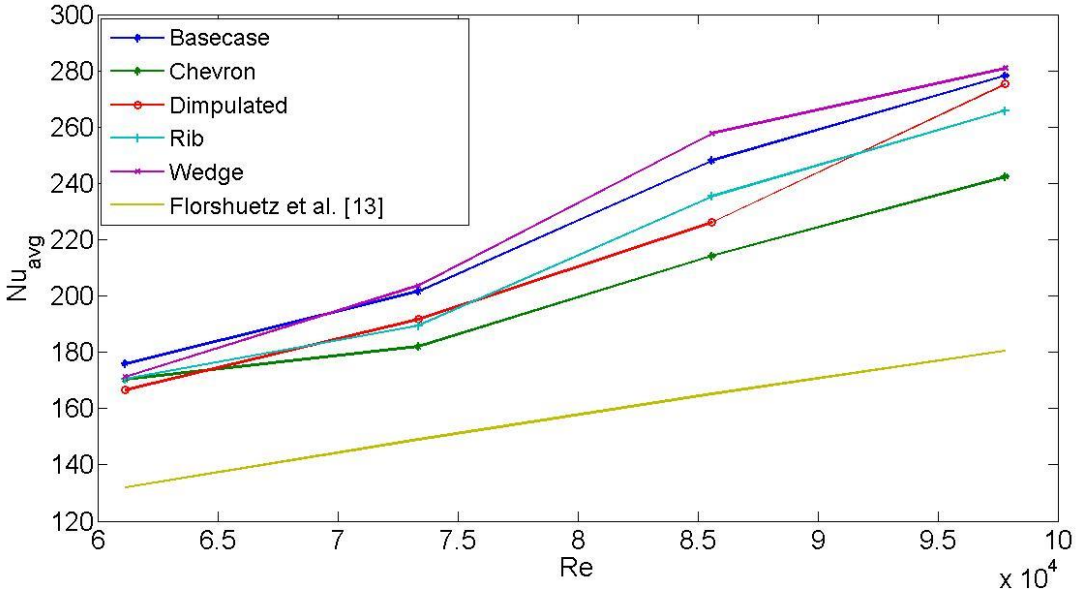

Figure 17. Total Averaged Heat Transfer Distribution

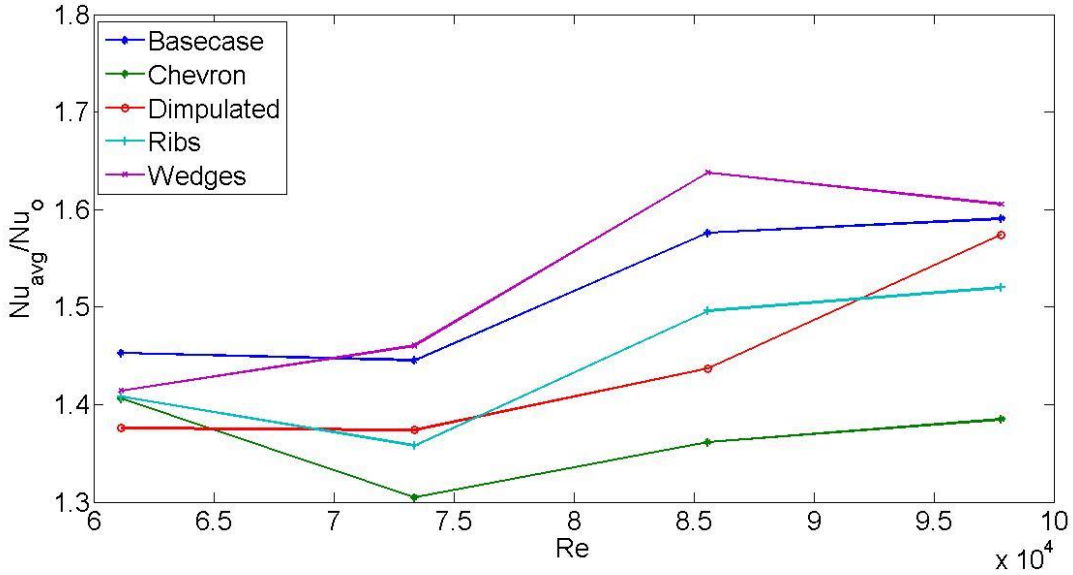

Figure 18. Total Averaged Heat Transfer Distribution Normalized by Nu_o

4.4 PRESSURE LOSS COEFFICIENT

The pressure drop for each configuration at varying Reynolds numbers used is illustrated in Figure 19. Unlike other internal cooling configurations using surface roughness, which generally the pressure loss tends to decrease proportionally with Re, the results illustrated in Figure 19 revealed an opposite trend. The pressure drops for the present configurations have been compared based on the friction factor, f, normalized by f_o, which is the friction factor obtained by the Petukhov correlation. The static pressure within the plenum was recorded during the experiments and the total pressure drop was calculated as the difference between this recorded pressure and the atmospheric pressure. The pressure loss within the entire channel is defined as dp/dx. The results revealed that the baseline case has the lowest pressure loss. Understandably, the presence of surface features like ribs, wedges and chevrons will impose greater resistance to the flow within the channel, leading to higher pressure loss. Thus, the pressure loss in these configurations is higher than that of the baseline case. The pressure loss in the configuration with dimples on the target plate is closer to the baseline case because there is no additional elements protruding into the flow field. The pressure loss of the case with ribs and wedge is comparable and approximately 30% higher than that of the baseline case. The pressure loss of the case with chevron elements and dimpulated surface is comparable to the baseline case at lower Re, but marginally higher, as the Re increases.

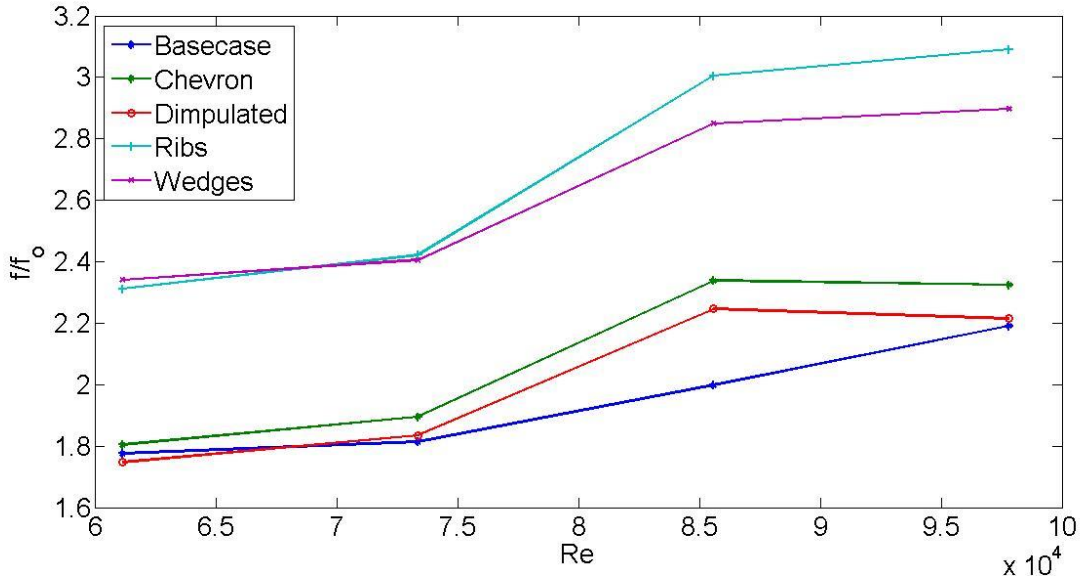

Figure 19. Pressure Loss Coefficient vs Re

4.5 NUMERICAL RESULTS

The numerical results were obtained for Re=73,000. The turbulence model used was SST and thus, the y+ values for all cases were < 2. A grid independence study was conducted with mesh of different sizes for all the configurations. The three mesh density used were 1.1 million, 2.2 million and 4.0 million in succession. The convergence criteria used are 10^{-5} for maximum RMS and a conservation criteria of 1% for all the equations. Additional monitor points are used at the target plate to monitor the fluctuations in the maximum and average value of the heat transfer. The predicted heat transfer results are higher for all the cases as compared to the experimental results. Qualitatively, the numerical results revealed favorable agreement compared to the experimental results. For all the cases, the numerical analysis with approximately 2.2 million

cells differed by 5% - 7% when compared to the cases with 4.0 million cells. Thus, mesh density with approximately 2.2 million cells was used to carry out the simulations in order to save computational time. Figure 20 shows both the experimental and numerical heat transfer distribution on the target plate for each configuration for Re = 73,000.

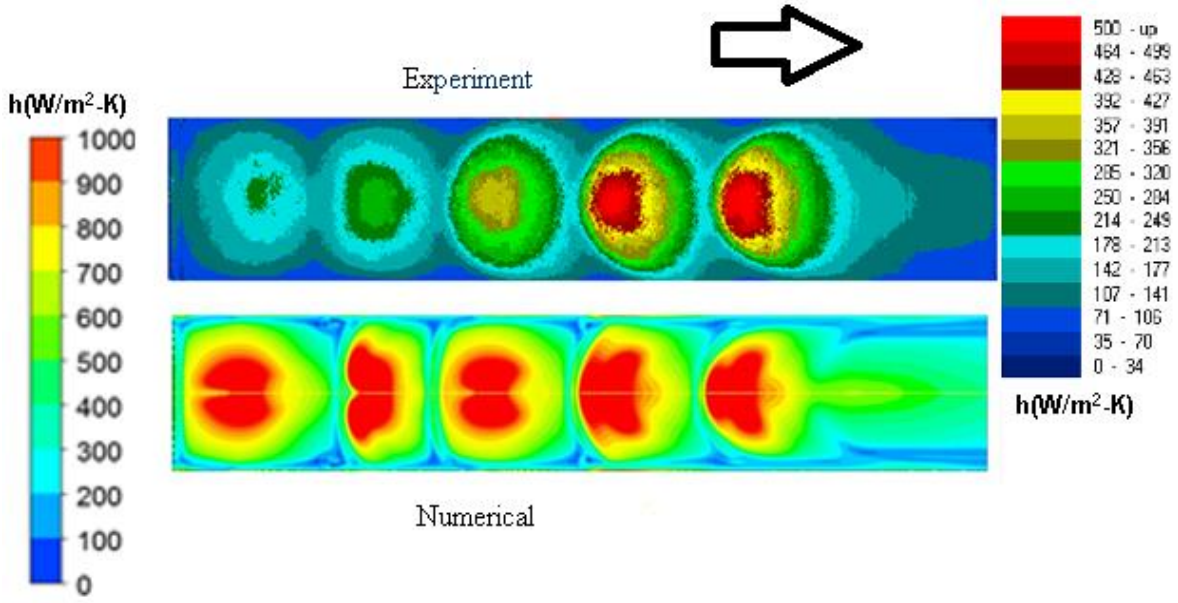

(a)

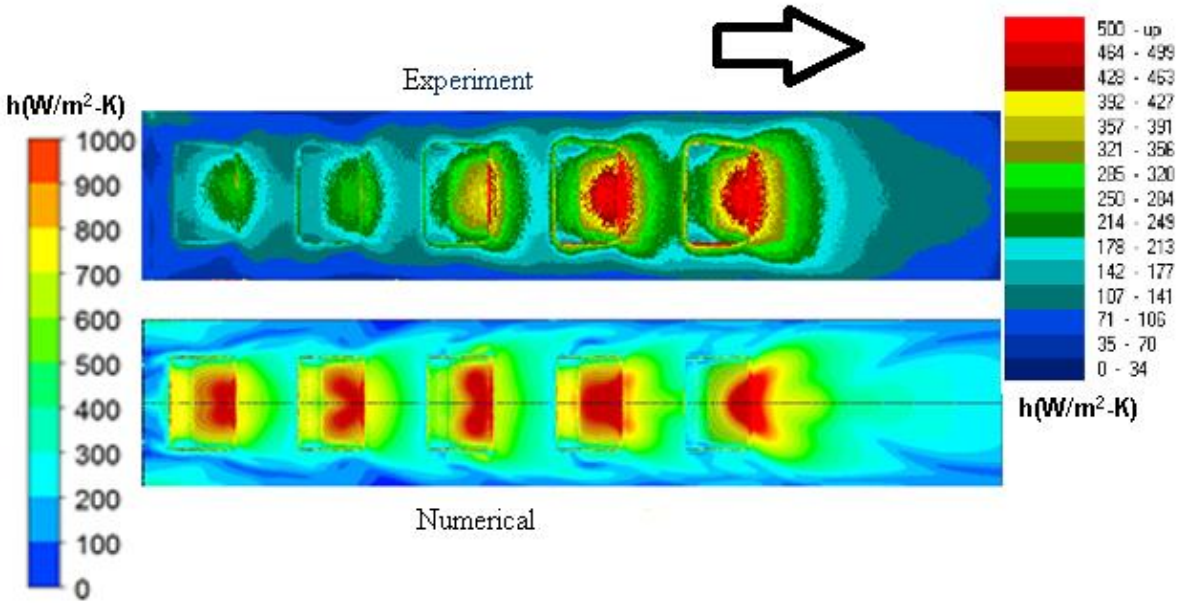

(b)

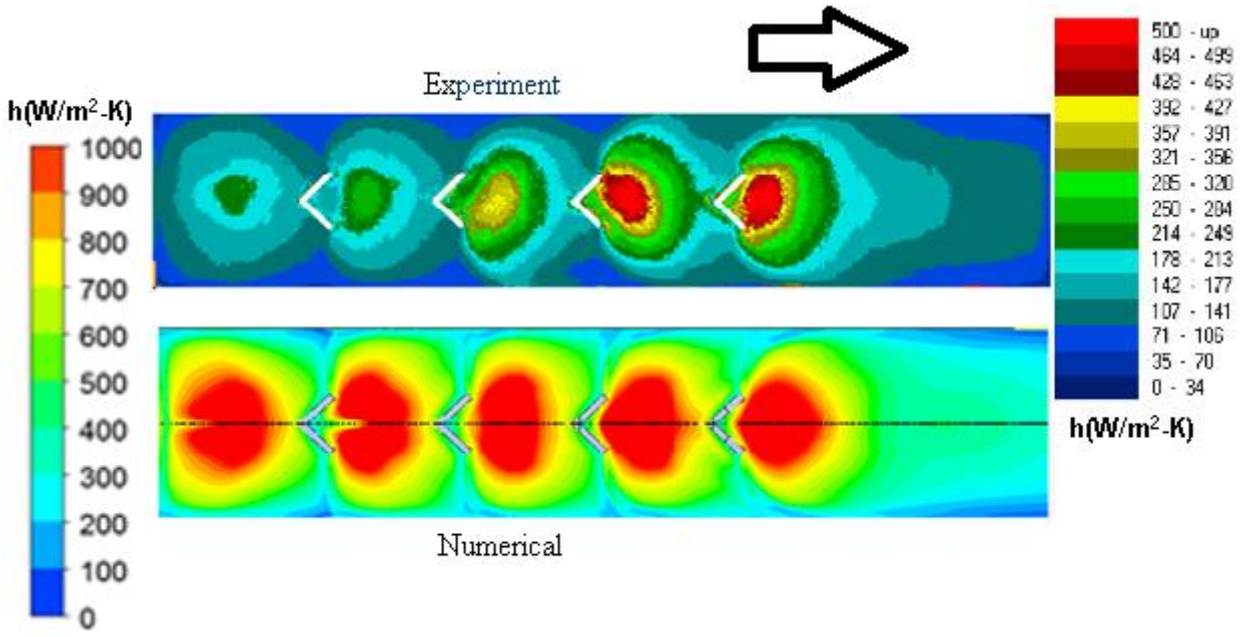
Experiment
h(W/m²-K)
1000
900
800
700
600
500
400
300
200
100
0
Numerical
500 - up
464 - 499
428 - 463
392 - 427
357 - 391
321 - 356
285 - 320
250 - 284
214 - 249
178 - 213
142 - 177
107 - 141
71 - 106
35 - 70
0 - 34
h(W/m²-K)

(c)

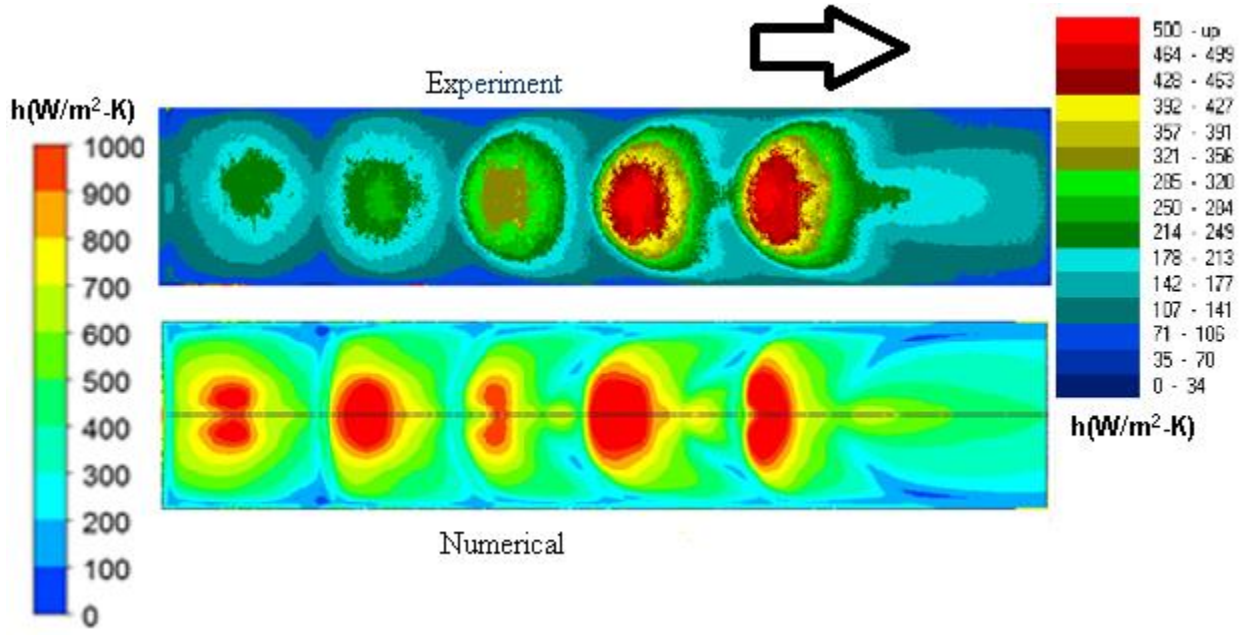
Experiment
h(W/m²-K)
1000
900
800
700
600
500
400
300
200
100
0
Numerical
500 - up
464 - 499
428 - 463
392 - 427
357 - 391
321 - 356
285 - 320
250 - 284
214 - 249
178 - 213
142 - 177
107 - 141
71 - 106
35 - 70
0 - 34
h(W/m²-K)

(d)

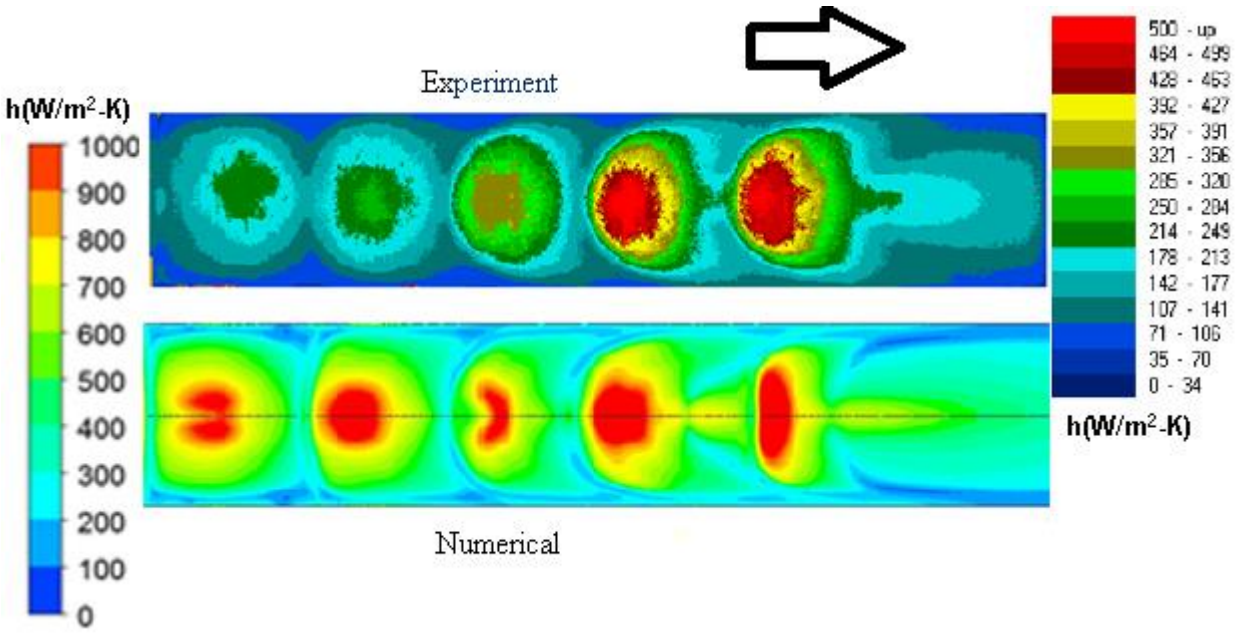

(e)

Figure 20. Comparison between Numerical and Experimental Heat Transfer Coefficient Distribution (a) Baseline Case (b) Dimpulate Target Plate (c) Chevron Elements (d) Ribs and (e) Wedges

The trend in the heat transfer distribution on the target plate as obtained in the experiments and numerical simulations have been compared in Figure 20. The distribution in the numerical simulations matches qualitatively with the distribution obtained in the experiments. However, the magnitude of the local heat transfer coefficients is overpredicted. There might be two possible reasons behind this 1) the use of SST turbulence model and 2) low quality of mesh generated. Due to lack of time, the mesh was generated using the ANSYS Workbench meshing tool. This tool does not have the flexibility and control of advanced meshing tools like ICEM and thus, the quality of individual elements in the mesh could not be strictly controlled. Specially, the prism elements in the inflation layer used to capture the boundary layer effects, had a high aspect ratio. However, the reason behind this over-prediction shall be addressed in the future. In the

following sections, the qualitative description of the flow field obtained by the simulations would be used to describe the trend obtained in the experiments.

The results in Figure 20 revealed that the numerical results for all configurations show higher heat transfer at the first and second jet compared to the experimental results. For the baseline case, the heat transfer pattern is largely comparable. At the first, second and third jets, the heat transfer is higher within the impingement zone and decreases radially. Towards the downstream, the heat transfer distribution is similar to that of a horseshoe vortex formation due to the presence of crossflow effects.

As can be seen, the numerical results correctly predicted the low heat transfer rates at the first two jets for all the configurations and an increase in the downstream impingement locations. This trend can also be observed in the experimental results. For the configuration with dimples on the target plates, the numerical simulation was able to capture the sudden increase in heat transfer at the edges of the dimples. The deflection of the stagnation point in the last jet also matches with that in the experimental result. For the configuration with the chevron elements, the numerical simulation is able to predict the low heat transfer regions located immediately downstream of the chevron elements between the chevron walls and corresponding jets. In case of the ribs and wedges, the heat transfer at the third jet is lower than the baseline case as already shown in the experimental results. Also, the enhancement in the downstream region near the exit is captured as well.

Figure 21 shows streamlines on the plane of symmetry of the flow domain while Figure 22 shows the streamlines on a plane located at a distance of H/4 from the target plate. From Figure 21 it can be seen that the velocity profile of the air coming out of the first two jets is skewed towards the downstream side. The velocity on the downstream side is higher than the

upstream side of the jet hole. The reason for this is that the first two inlets in the plenum used for the experiments overlap with the first two jet holes in the jet plate. As a result, the high speed flow entering through the first two plenum inlet ports partially enter the first two jet holes directly. This high speed flow directly entering the jet holes distorts the jet inlet velocity and pressure profile. This causes the core to weaken and thus, the heat transfer at the target plate is lower at Jet 1 and Jet 2 is lower. This condition exists for all the configurations as the same plenum was used throughout the study.

As can be seen in Figure 21 (b), after impingement, the radially expanding flow within the dimple cavity is pushed out in a direction perpendicular to the target wall. This causes flow separation at the edges of the dimples which form vortices on interacting with the radially expanding air from the upstream jets. This mixing and enhancement in turbulence causes a high local heat transfer on the edges. With the development of the crossflow jets 3, 4 and 5 start deflecting in the downstream direction. As a result the stagnation point shifts more towards the downstream edge and a higher heat transfer is observed.

For the chevron elements, Figure 21(c), a large recirculation zone is observed just downstream of the chevrons which forms a low heat transfer region. This is because the radially spreading jet interacts with the chevron walls and is turned away from the target wall along the height of the chevron elements. Negligible deflection of the jets is observed in this configuration because the crossflow is deflected away from the jets as can be seen in Figure 22.

The ribs, Figure 21(d), and wedges, Figure 21(e), deflect the crossflow towards the target plate and hence, the jets get a greater chance to develop before impinging on the target plate. The spreading air from two adjacent jets interact to form vortices similar to the baseline case. But due to the presence of ribs and wedges and an increase in crossflow near the target plate caused by

them, these vortices are reduced in size and the stagnation point is deflected further downstream. The jets adjacent to the wedges face a greater deflection as compared to the jets adjacent to ribs. This is again due to the increase in the crossflow which is also evident from Figure 22.

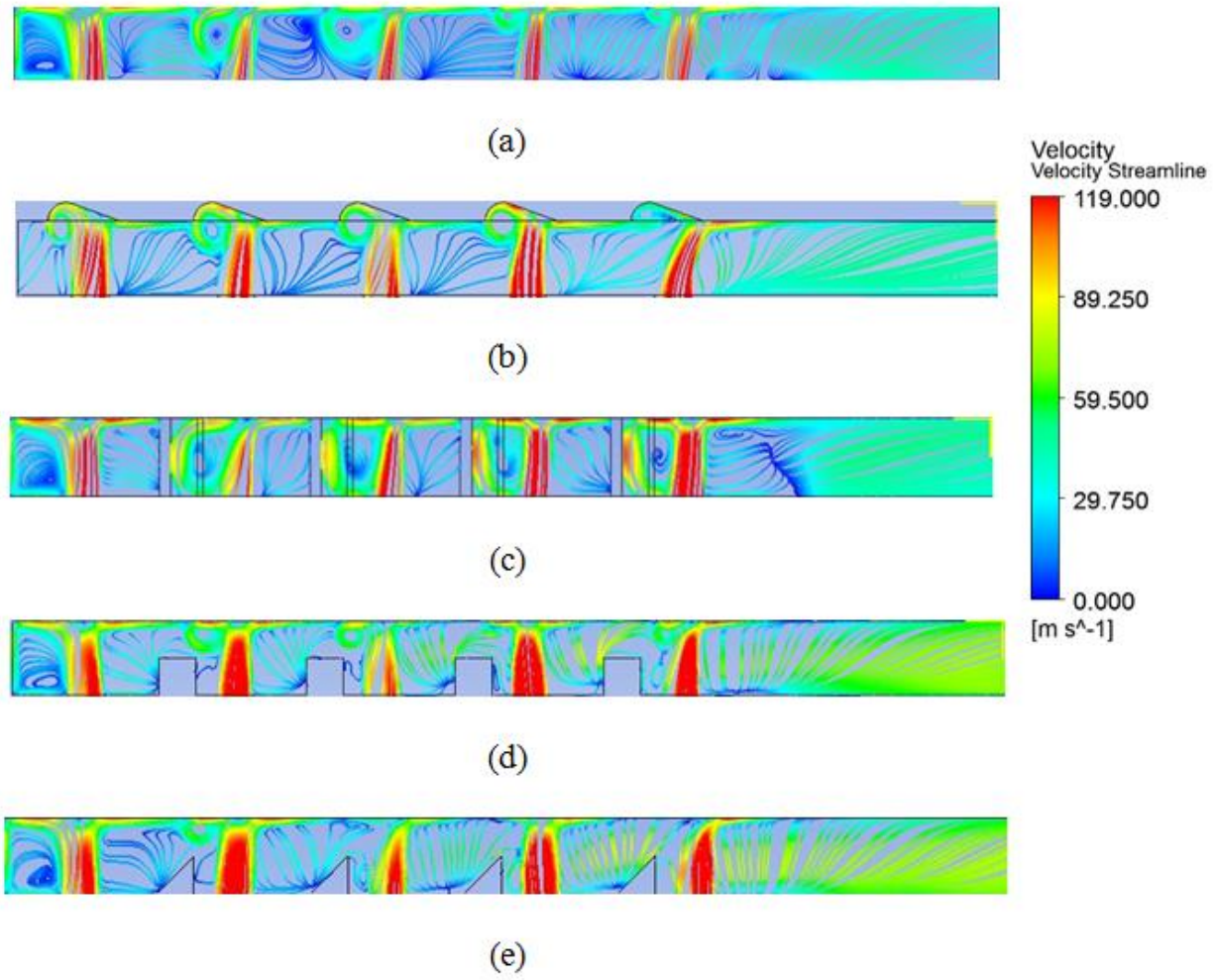

Figure 21. Streamwise Velocity Profile for Re = 73,000 (a) Baseline Case (b) Dimpulated Target Plate (c) Chevron Elements (d) Ribs and (e) Wedges

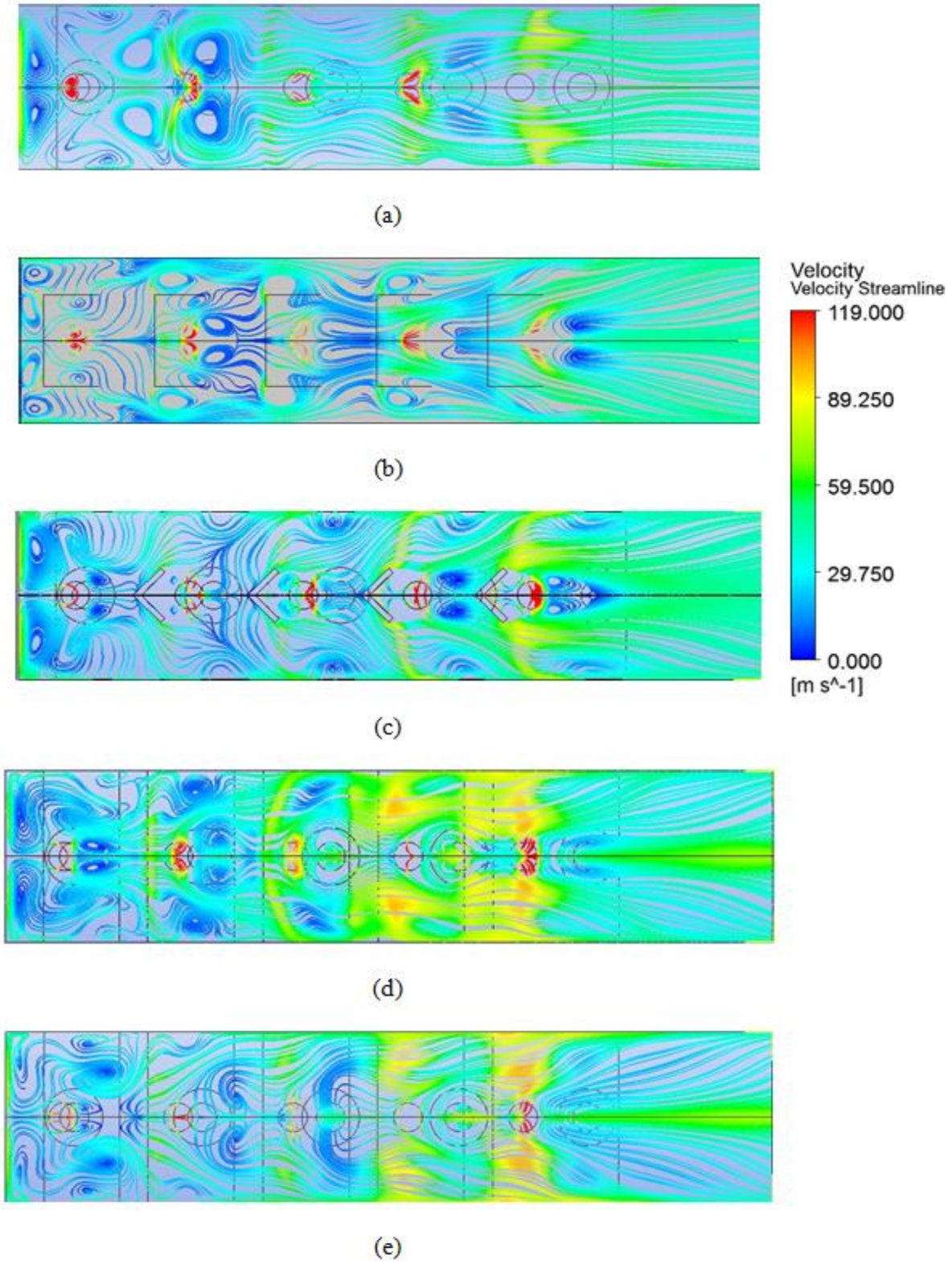

Figure 22. Streamwise Velocity Profile for Re = 73,000 (a) Baseline Case (b) Dimpulated Target Plate (c) Chevron Elements (d) Ribs and (e) Wedges

5.0 CONCLUSIONS

In the present study, four different surface features designed for a plenum fed narrow jet impingement channel with H/D = 2, were tested using transient liquid crystal technique and numerical analysis through computational fluid dynamics (CFD) to evaluate their potential to enhance heat transfer. The experiments were carried out for four different Reynolds number of 61,000, 73,000, 85000 and 97,000 which was based on the jet diameter which remained constant for all the test sections. The enhancement in the heat transfer were lower than expected. This is because this study provided first set of data and there is a need for optimization of the geometries which could not be done due to a time constraint. However, the findings gave an insight into the flow field features and type of heat transfer distribution observed for these novel features. The experimental results showed that the 45^{o} wedges gave the highest total averaged heat transfer enhancement as compared to other geometries. The maximum enhancement obtained in the total averaged heat transfer was approximately 4 % over the baseline case. Both ribs and wedges showed higher heat transfer in the downstream direction because they were able to deflect a greater amount of coolant towards the target plate. Also, the wedges and the ribs provided some protection to the jets against the crossflow. On the other hand, they caused deflection of the jets before impingement by diverting more high speed coolant towards the target plate.

The dimpulated and chevron test sections have a lower heat transfer because they restricted the spreading of the jets on the impingement surface causing a non-uniform heat

transfer coefficient distribution. This led to a lower total averaged values for these configurations. However, the numerical results showed that the chevrons were very successful in minimizing the effect of the crossflow on the jets and hence, a negligible deflection of the jets was observed.

The ribs and wedges showed the highest pressure drop of approximately 30%. On the other hand, the dimpulated and chevron test sections exhibited a pressure drop very similar to the baseline case. Thus, with slight optimization, higher enhancement in heat transfer should be possible for a moderate pressure drop penalty.

It was observed that the heat transfer was lower near the first and second jets and increased in the downstream direction. The lower heat transfer in the first and second jets was attributed to the weak nature of these jets. As shown in the numerical findings, the plenum inlet jets impinged very close to the first two jet holes on the jet issuing plate altering the flow field at the entry of the first and second jets, altering the velocity and pressure distribution which ultimately weakened these jets. This trend was observed in all the test cases since, the same plenum was used for all the experiments. Another plausible cause for higher heat transfer in the downstream direction could be the decrease in the static pressure in the channel as the flow moves downstreams.

The numerical results showed good qualitative agreement with the experimental results. Using these results, a better insight into the flow field existing in each configuration was obtained. This helped in understanding the factors that influenced the observed heat transfer distributions which could be further utilized for optimization studies.

5.1 FUTURE WORKS

The experimental and numerical work described in the present study provided a first set of data regarding the heat transfer performance of four novel surface features designed for a narrow impingement channel. Although, there was no appreciable improvement in the heat transfer, but an insight into the flow field existing in the different configurations was obtained which could be related to the heat transfer behavior observed. But due to time constraint, no optimization study could be performed, which could have helped in improving the overall performance.

1. As shown in the numerical findings, the design of the plenum affected the flow field in the first and second jets. The compressed air supply entering the plenum formed a jet which impinged on the plenum side surface of the jet plate and very close to the entry of the first and second jet holes. Ideally, the flow in the plenum should have very low velocities. This can be achieved by redesigning the experimental setup and incorporating a vacuum pump which could be attached to the exit side of the test sections. This would ensure a low speed flow within the plenum.
2. As seen in the results, the dimples restricted the radial spread of the impinging jets which negatively affected the heat transfer performance. However, very high heat transfer regions were detected near the dimple edges. Thus, in the next phase of study, the dimples with optimized surface area can be explored, so that they do not restrict the radial flow which is important for achieving a uniform heat transfer. An optimization study for the edges could also be done to help in reducing the extent of flow separation.
3. The chevron elements were able to reduce the effect of the crossflow to a great extent, but restricted the radial flow of the impinging jets. This was the main cause behind their low heat transfer performance. Thus, shorter chevron elements, which do not touch the target surface,

can be studied. This would allow the impinging jets to expand without any restriction and a more uniform heat transfer distribution can be achieved. This coupled with the ability of the chevrons to reduce deflection could lead to a higher heat transfer enhancement. Apart from this, the distance between the chevron elements and jets could be varied in order to reduce the size of the recirculation zones. Additionally, because the crossflow increases in velocity in the downstream direction, an array of chevrons with varying distance from the jets in downstream direction could give an optimized performance

4. In the current study, ribs and wedges with constant dimensions were tested. The variation in the dimensions, specially, in the height of these features can change the amount of crossflow being diverted towards the target plate. Thus, ribs and wedges with varying heights and inclination angles could be explored next. Again, the upstream distance between these elements and the jets is an important factor and an optimization study for this parameter can be performed.

BIBLIOGRAPHY

[1] Martinez-Frias, J., Aceves, S. M., Ray Smith, J., and Brandt, H., 2008, "A Coal-Fired Power Plant with Zero-Atmospheric Emissions," Journal of Engineering Gas Turbines Power, **130**(2), pp. 023005–023005.

[2] Rao, A., "1.3.2. Advanced Brayton Cycles", http://www.netl.doe.gov/research/coal/energy-systems/turbines/publications/handbook

[3] Han, J.-C., Dutta, S., and Ekkad, S., 2012, "Gas Turbine Heat Transfer and Cooling Technology", Second Edition, CRC Press, Boca Raton, FL.

[4] Terzis, A., Cochet, M., von Wolfersdorf, J., Weigand, B., and Ott, P., 2014, "Detailed Heat Transfer Distributions of Narrow Impingement Channels with Varying Jet Diameter," Proceedings of ASME Turbo Expo 2014: Turbine Technical Conference and Exposition, (GT2014-25910), pp. 1–11.

[5] Lafleur, R. S., "Method for Cooling a Wall within a Gas Turbine Engine.", European Patent EP 1 617 043 B1, dated Jun. 11, 2008.

[6] Matthew A. Devore, Corneil S. PaauWe, "Turbine Airfoil with Improved Cooling", US Patent 7,600,966, B2, dated Oct. 13, 2009.

[7] George Liang, "Blade For A Gas Turbine",US Patent 7,819,629, B2, dated Oct 26, 2010.

[8] Christian X. Campbell, Jay A- Morrlson, "Turbine Airfoil with a Compliant Outer Wall", US Patent 8,147,196, B2, dated Apr. 3, 2012.

[9] George Liang, "Light Weight and Highly Cooled Turbine Blade", US Patent 8,057,183, B1, dated Nov. 15, 2011.

[10] Chyu, M.K. and Alvin, M.A., "Turbine Airfoil Aerothermal Characteristics in Future Coal–Gas-Based Power Generation Systems", Heat Transfer Research 41 (7) (2010) 737–752.

[11] Bunker, R. S., 2013, "Gas Turbine Cooling: Moving from Macro to Micro Cooling."ASME Turbo Expo 2013: Turbine Technical Conference and Exposition, pp. V03CT14A002-V03CT14A002.

[12] O'Donovan, T. S., and Murray, D. B., 2007, "Jet Impingement Heat Transfer – Part I: Mean and Root-Mean-Square Heat Transfer and Velocity Distributions," International Journal of Heat and Mass Transfer, **50**(17–18), pp. 3291–3301.

[13] Weigand, B., and Spring, S., 2011, "Multiple Jet Impingement - A Review," Heat Transfer Research, **42**(2), pp. 101–142.

[14] Downs, S. J., and James, E. H., 1987, "Jet Impingement Heat Transfer - A Literature Survey," ASME, AIChE, and ANS, 24th National Heat Transfer Conference and Exhibition.

[15] Obot, N. T., and Trabold, T. A., 1987, "Impingement Heat Transfer within Arrays of Circular Jets: Part 1—Effects of Minimum, Intermediate, and Complete Crossflow for Small and Large Spacings," Journal of Heat Transfer, **109**(4), p. 872.

[16] Kenneth W. Van Treuren, Zoulan Wang, Peter T. Ireland, and Terry V. Jones, 1994, "Local Heat Transfer Coefficient and Adiabatic Wall Temperature Measurement beneath Arrays of Staggered and Inline Impinging Jets," International Gas Turbine and Aeroengine Congress and Exposition, 94-GT-181.

[17] Kercher, D. M., and Tabakoff, W., 1970, "Heat Transfer by a Square Array of Round Air Jets Impinging Perpendicular to a Flat Surface Including the Effect of Spent Air," Journal of Engineering for Power, **92**(1), pp. 73–82.

[18] Hollworth, B. R., and Cole, G. H., 1987, "Heat Transfer to Arrays of Impinging Jets in a Crossflow," Journal of Turbomachinery, **109**(4), pp. 564–571.

[19] Florschuetz, L. W., Truman, C. R., and Metzger, D. E., 1981, "Streamwise Flow and Heat Transfer Distributions for Jet Array Impingement with Crossflow," Journal of Heat Transfer, **103**(2), pp. 337–342.

[20] Chambers, A. C., Gillespie, D. R. H., Ireland, P. T., and Dailey, G. M., 2005, "The Effect of Initial Cross Flow on the Cooling Performance of a Narrow Impingement Channel," Journal of Heat Transfer, **127**(4), pp. 358–365.

[21] Terzis, A., Wagner, G., von Wolfersdorf, J., Ott, P., and Weigand, B., 2014, "Hole Staggering Effect on the Cooling Performance of Narrow Impingement Channels using the Transient Liquid Crystal Technique," Journal of Heat Transfer, **136**(7), p. 071701.

[22] Park, J., Goodro, M., Ligrani, P., Fox, M., and Moon, H.-K., 2007, "Separate Effects of Mach Number and Reynolds Number on Jet Array Impingement Heat Transfer," Journal of Turbomachinery, **129**(2), pp. 269–280.

[23] El-Gabry, L. A., and Kaminski, D. A., 2005, "Experimental Investigation of Local Heat Transfer Distribution on Smooth and Roughened Surfaces under an Array of Angled Impinging Jets," Journal of Turbomachinery, **127**(3), pp. 532–544.

[24] Miller, N., Siw, S.C., Chyu, M.K. and Alvin, M.A., 2013. "Optimization of Single Row Jet Impingement Array by Varyin Flow Rates.", Proceedings of ASME Summer Heat Transfer Conference, HT2013-17342, July 14-19

[25] Liu, Y.-H., Song, S.-J., and Lo, Y.-H., 2013, "Jet Impingement Heat Transfer on Target Surfaces with Longitudinal and Transverse Grooves," International Journal of Heat and Mass Transfer, **58**(1–2), pp. 292–299.

[26] Baughn, J. W., Ireland, P. T., Jones, T. V., and Saniei, N., 1989, "A Comparison of the Transient and Heated-Coating Methods for the Measurement of Local Heat Transfer Coefficients on a Pin Fin," Journal of Heat Transfer, **111**(4), pp. 877–881.

[27] Critoph, R.E., and Fisher, M., 1998, "A Study of Local Heat Transfer Coefficients in Plate Fin-Tube Heat Exchangers Using the Steady State and Transient Liquid Crystal Techniques," IMECHE Conference Transactions, Vol. 2, pp. 201-210.

[28] Yen, C.-H. (Erik), 1999, "An Experimental Study of Heat Transfer Around Turbine Airfoils with Closed-Loop Cooling", ProQuest Dissertations and Theses; Thesis (Ph.D.), Carnegie Mellon University, 1999.

[29] Ekkad, S. V., and Han, J.-C., 2000, "A Transient Liquid Crystal Thermography Technique for Gas Turbine Heat Transfer Measurements," Measurement Science and Technology., **11**(7), p. 957.

[30] Kline, S.J. and McClintock, F.A., "Describing Uncertainties in Single Sample Experiments," Engineering (The American Society of Mechanical Engineers), 75, pp. 3-8.

[31] Zu, Y. Q., Yan, Y. Y., and Maltson, J. D., 2009, "CFD Prediction for Multi-Jet Impingement Heat Transfer," Proceedings of ASME Turbo Expo 2009: Power for Land, Sea, and Air, **3**: Heat Transfer, Parts A and B, (GT2009-59488) pp. 483-490.

[32] Rao, G. A., Kitron-Belinkov, M., and Levy, Y., 2009, "Numerical Analysis of a Multiple Jet Impingement System," Proceedings of ASME Turbo Expo 2009: Power for Land, Sea, and Air, **3**: Heat Transfer, Parts A and B, (GT2009-59719) pp. 629–639.

[33] Goldstein, R. J., and Seol, W. S., 1991, "Heat Transfer to a Row of Impinging Circular Air Jets Including the Effect of Entrainment," International Journal of Heat and Mass Transfer, **34**(8), pp. 2133–2147.

[34] Wan, C., Rao, Y., and Chen, P., 2015, "Numerical Predictions of Jet Impingement Heat Transfer on Square Pin-Fin Roughened Plates," Applied Thermal Engineering, **80**, pp. 301–309.

[35] Taslim, M. E., and Bethka, D., 2009, "Experimental and Numerical Impingement Heat Transfer in an Airfoil Leading-Edge Cooling Channel With Cross-Flow," Journal of Turbomachinery, **131**(1), p. 011021.

[36] Xing, Y., and Weigand, B., 2013, "Optimum Jet-to-Plate Spacing of Inline Impingement Heat Transfer for Different Crossflow Schemes," Journal of Heat Transfer, **135**(7), p. 072201.

[37] Lee, J., Ren, Z., Haegele, J., Potts, G., Sik Jin, J., Ligrani, P., Fox, M. D., and Moon, H.-K., 2013, "Effects of Jet-To-Target Plate Distance and Reynolds Number on Jet Array Impingement Heat Transfer," Journal of Turbomachinery, **136**(5), p. 051013.

[38] Terzis, A., Ott, P., von Wolfersdorf, J., Weigand, B., and Cochet, M., 2014, "Detailed Heat Transfer Distributions of Narrow Impingement Channels for Cast-In Turbine Airfoils," Journal of Turbomachinery, **136**(9), p. 091011.

[39] Hammad, K. J., and Milanovic, I. M., 2009, "Flow Structure in the Near-Wall Region of a Submerged Impinging Jet," ASME, pp. 1445–1455.

[40] Ligrani, P., 2013, "Heat Transfer Augmentation Technologies for Internal Cooling of Turbine Components of Gas Turbine Engines," International Journal of Rotating Machinery, **2013**, pp. 1–32.

[41] Zuckerman, N., and Lior, N., 2005, "Impingement Heat Transfer: Correlations and Numerical Modeling," Journal of Heat Transfer, **127**(5), pp. 544–552.